(12)

DTNSRDC-82/063

DAVID W. TAYLOR NAVAL SHIP RESEARCH AND DEVELOPMENT CENTER

Bethesda, Maryland 20084

SUPERCAVITATING PROPELLERS–DESIGN THEORY AND EXPERIMENTAL EVALUATION

AD A123518

SUPERCAVITATING PROPELLERS–DESIGN THEORY AND EXPERIMENTAL EVALUATION

by

B. Yim
G. Larimer
J. Peck

APPROVED FOR PUBLIC RELEASE: DISTRIBUTION UNLIMITED

SHIP PERFORMANCE DEPARTMENT
RESEARCH AND DEVELOPMENT REPORT

January 1983

DTNSRDC-82/063

MAJOR DTNSRDC ORGANIZATIONAL COMPONENTS

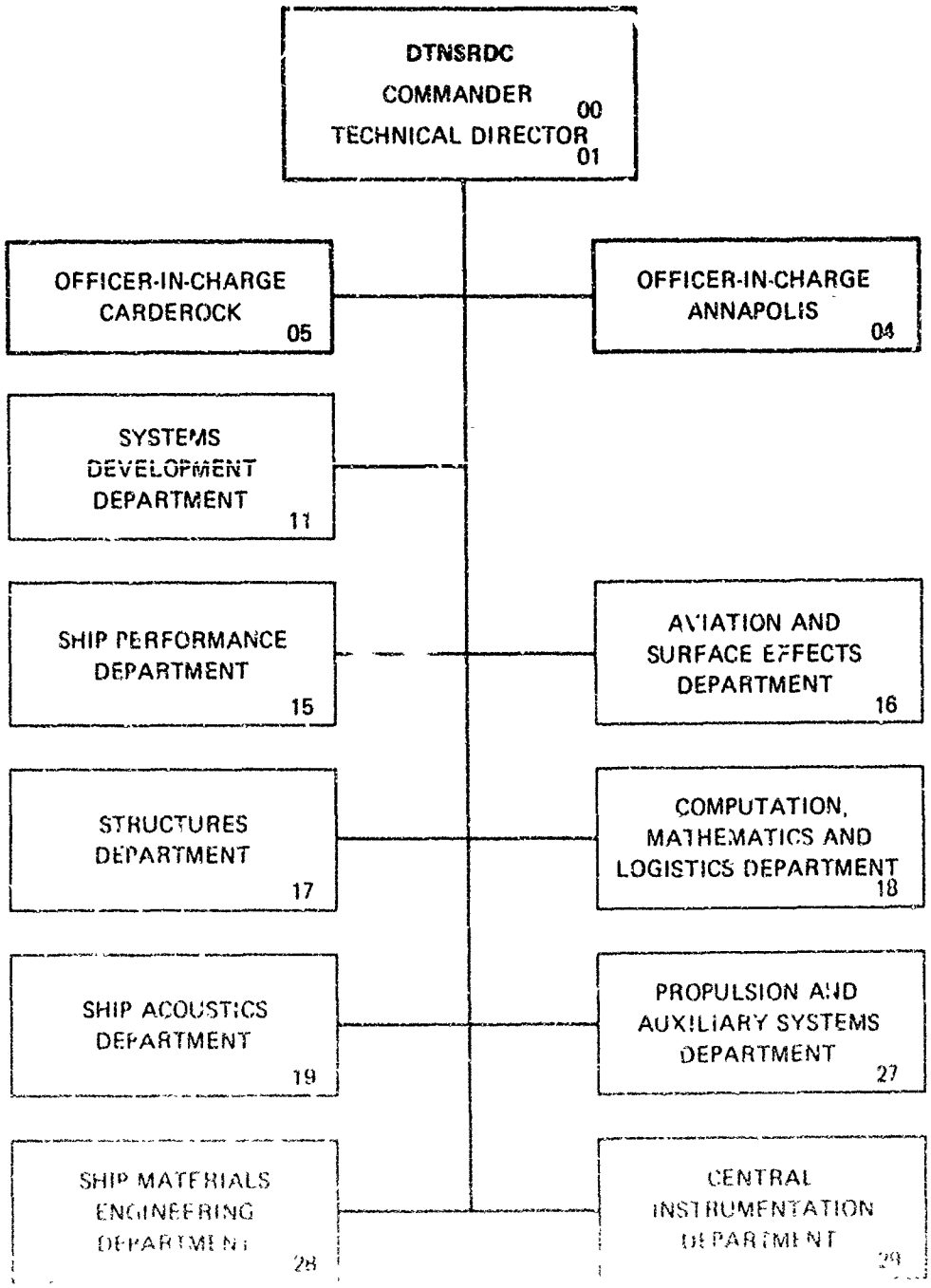

UNCLASSIFIED

SECURITY CLASSIFICATION OF THIS PAGE *(When Data Entered)*

REPORT DOCUMENTATION PAGE		READ INSTRUCTIONS BEFORE COMPLETING FORM
1. REPORT NUMBER DTNSRDC-82/068	2. GOVT ACCESSION NO. AD-A123518	3. RECIPIENT'S CATALOG NUMBER
4. TITLE *(and Subtitle)* SUPERCAVITATING PROPELLERS--DESIGN THEORY AND EXPERIMENTAL EVALUATION		5. TYPE OF REPORT & PERIOD COVERED Research and Development 6. PERFORMING ORG. REPORT NUMBER
7. AUTHOR(s) B. Yim, G. Larimer and J. Peck		8. CONTRACT OR GRANT NUMBER(s)
9. PERFORMING ORGANIZATION NAME AND ADDRESS David W. Taylor Naval Ship Research and Development Center Bethesda, Maryland 20084		10. PROGRAM ELEMENT, PROJECT, TASK AREA & WORK UNIT NUMBERS (See reverse side)
11. CONTROLLING OFFICE NAME AND ADDRESS Naval Material Command Naval Sea Systems Command		12. REPORT DATE January 1983 13. NUMBER OF PAGES 98
14. MONITORING AGENCY NAME & ADDRESS*(if different from Controlling Office)*		15. SECURITY CLASS. *(of this report)* UNCLASSIFIED 15a. DECLASSIFICATION/DOWNGRADING SCHEDULE

16. DISTRIBUTION STATEMENT *(of this Report)*

APPROVED FOR PUBLIC RELEASE: DISTRIBUTION UNLIMITED

17. DISTRIBUTION STATEMENT *(of the abstract entered in Block 20, if different from Report)*

18. SUPPLEMENTARY NOTES

19. KEY WORDS *(Continue on reverse side if necessary and identify by block number)*

Lifting Surface Theory
Numerical Procedures
Supercavitating Propeller
Propeller Design

20. ABSTRACT *(Continue on reverse side if necessary and identify by block number)*

A lifting-surface theory and numerical procedure for designing supercavitating propellers are presented.

Both a subcavitating and a supercavitating propeller are represented by vortex and source distributions. Unlike the subcavitating propeller, however, source strengths for a supercavitating propeller are related to cavity thickness, which is not known without examination, and have to be

(Continued on reverse side)

DD FORM 1 JAN 73 1473 EDITION OF 1 NOV 65 IS OBSOLETE
S/N 0102-LF-014-6601

UNCLASSIFIED

SECURITY CLASSIFICATION OF THIS PAGE *(When Data Entered)*

(Block 10)

Program Element 62543N
Task Area ZF43421001
Work Units 1500-103 and 1542-817

(Block 20 continued)

obtained by solving related integral equations. Numerical solution of the integral equations is obtained as a correctional function for a stripwise supercavitating cascade theory which, with lifting-line theory, is used for preliminary design of supercavitating propellers. The induced axial, radial, and tangential velocities are obtained on a blade reference surface that allows arbitrary skew, rake, and radial pitch variations. The blade shape is obtained as a correction to the shape obtained from stripwise supercavitating cascade theory. Thrust and torque coefficients are obtained from pressures on the blade surface.

The method is applied in designing several supercavitating propellers that have design conditions the same as those of existing supercavitating propellers.

Numerical computations were also used to design two additional supercavitating propellers which were built and tested. The design predictions are compared to the experimental data, both for blade cavity height and performance characteristics, and good correlation is obtained.

Accession For	
NTIS GRA&I	☑
DTIC TAB	☐
Unannounced	☐
Justification	
By	
Distribution/	
Availability Codes	
Dist	Avail and/or Special
A	

TABLE OF CONTENTS

LIST OF FIGURES

LIST OF TABLES

NOTATION

A_{ij}	Coefficients of simultaneous equations defined in Equation (36)
B	Expression defined by Equation (13)
C_{bv}	Frictional drag coefficient
C_D	Drag coefficient; drag divided by $1/2\ \rho\ V_s^2$
C_{Dc}	Cavity drag coefficients
C_p	Power coefficient = $\omega Q/(\pi/2\rho V_s^3 R^2)$
C_T	Thrust coefficient = $\tau/(\pi/2\rho V_s^2 R^2)$
c	Chord length divided by propeller radius
c_o	Camber correction factor
D	Propeller diameter
EAR	Expanded area ratio
H	Expression defined by Equation (14)
H_1	Quantities defined by Equation (20-1)
J	Advance coefficient: $V_A/(nD)$
K_Q	Torque coefficient: $Q/(\rho n^2 D^5)$
K_T	Thrust coefficient: $T/(\rho n^2 D^4)$
ℓ	Cavity length divided by the chord length
n	Revolutions per second, rps
P	Pressure
P/D	Pitch-diameter ratio
p	Nondimensional perturbation pressure $(P-P_\infty)/1/2\rho V_s^2)$

Q	Torque
R	Propeller radius
R_n	Reynolds number
r,θ,x	Cylindrical coordinate system defined in Figure 1
r_H	Hub radius divided by the propeller radius
T	Thrust
u_T^m	Tangential component of perturbation velocity caused by source distribution
V_A	Speed of advance: $V_s(1-w)$
V_s	Ship speed
w	Wake fraction
x,y,z	Local rectangular coordinate system
Z	Blade number
α	Angle of attack of blade section
β	Geometric pitch angle
β_i	Hydrodynamic pitch angle
Γ	Strength of nondimensional circulation
δ_k	Quantity defined by Equation (14)
η	Propeller efficiency
λ	$r \tan \beta_i$
ξ,η,ζ	Local rectangular, coordinate system
ρ,ϕ,ξ	Cylindrical coordinate system defined in Figure 1
ρ	Mass density of water
σ	Cavitation number
ω	Angular speed

Superscript

G	Velocities caused by vortices
m	Velocities caused by sources

Subscript

c	On cavity
ℓ	Local
n	Normal direction
T	Tangential direction

ABSTRACT

A lifting-surface theory and numerical procedure for designing supercavitating propellers are presented.

Both a subcavitating and a supercavitating propeller are represented by vortex and source distributions. Unlike the subcavitating propeller, however, source strengths for a supercavitating propeller are related to cavity thickness, which is not known without examination, and have to be obtained by solving related integral equations. Numerical solution of the integral equations is obtained as a correctional function for a stripwise supercavitating cascade theory which, with lifting-line theory, is used for preliminary design of supercavitating propellers. The induced axial, radial, and tangential velocities are obtained on a blade reference surface that allows arbitrary skew, rake, and radial pitch variations. The blade shape is obtained as a correction to the shape obtained from stripwise supercavitating cascade theory. Thrust and torque coefficients are obtained from pressures on the blade surface.

The method is applied in designing several supercavitating propellers that have design conditions the same as those of existing supercavitating propellers.

Numerical computations were also used to design two additional supercavitating propellers which were built and tested. The design predictions are compared to the experimental data, both for blade cavity height and performance characteristics, and good correlation is obtained.

ADMINISTRATIVE INFORMATION

The Naval Material Command (NAVMAT 08T) funded this investigation in support of an ongoing Ship Performance and Hydromechanics Exploratory Development Program (Program Element 62543N, Task Area ZF43421001) assigned to the David W. Taylor Naval Ship Research and Development Center (the Center). This work has been completed under the High-Speed Propulsor Task portion of this program, (Center Work Unit 1500-103), and partly under the Naval Sea Systems Command's General Hydrodynamic Research Program (Center Work Unit 1542-817).

INTRODUCTION

Ever since supercavitating propellers were first investigated systematically,[1,2*] steady progress has been made in understanding associated problems.[3,4] Designers of supercavitating propellers have been urged to consider the interference

*A complete listing of references is given on page 83.

effect of neighboring cavities and the effect of flow retardation.[2,4] To this end, three-dimensional cavity-flow theory similar to the lifting-surface theory for subcavitating propellers[5,6] has been formulated.[7-10] However, to date none of the theories has been applied to the actual design of a supercavitating propeller owing to the numerical complexity of the problem.

As with subcavitating propellers,[5] a supercavitating propeller may be designed in two steps: preliminary or lifting-line design and final or lifting-surface design. The former gives an approximate solution and supplies basic data to the latter. The preliminary design supplies information for the final design concerning load distribution on the blade and preliminary pitch distribution, which forms the basic singularity surface for the final design. The section shape of the blade cavity and the cavity length of a supercavitating cascade model are also computed in the preliminary design. The information is used in the final design as the first approximation. Although this report deals mainly with the final design, we also consider aspects of the preliminary design[11] to help the reader understand the final design more fully.

The propeller diameter, the blade number and contour, the hub diameter for the given propeller-thrust power coefficient with the given ship speed, propeller revolutions per minute (rpm), and the wake fraction are considered to have been determined before applying the present preliminary and final programs. To ensure that the designed propeller is fully cavitating and that the blades are thick enough, the leading-edge cavity thickness is specified. If the specified cavity thickness near the leading edge does not accommodate a stable cavity of at least 1.5 chord lengths because the cavitation number is too large, then the leading-edge cavity thickness is increased internally to make a long enough cavity for the preliminary program.

The purpose of the present program is to design a fully cavitating propeller that is efficient, has no face cavitation, is structurally strong, and meets the design requirements.

As for a subcavitating propeller, the supercavitating propeller is represented by vortex and source distributions.[6] The source strengths are related to the cavity thickness, are not known a priori and are to be obtained by solving related singular integral equations. When the source strengths are known, the supercavitating propeller problem is similar to the problem for a subcavitating propeller with thick and wide blades. Thus, many of the computation techniques apply to both

subcavitating[5,6] and supercavitating propellers. Indeed, this present study makes use of many parts of the lifting-surface design programs reported by Kerwin[6] for a subcavitating propeller. The coordinate systems of the blade are the same for both propeller types.

Since the singular integral equation is a Fredholm equation of the first kind, the method for its solution must be chosen with extreme care. Additionally, the cavity shape is not known without examination. Thus, iteration and/or some special cavity model has to be applied knowing that all the inviscid cavity models are not exact; rather, they are approximate representations. The source distribution is obtained from a stripwise, two-dimensional, supercavitating-cascade representation developed in the preliminary design. For the procedure used at present, the source distribution is multiplied by a double polynomial having unknown coefficients in terms of the radial and chordwise coordinates. Since the two-dimensional cavity model used in preliminary design is a linear, double spiral vortex model, the cavity streamline is closed at infinity instead of at the cavity end. Thus the unknown source strengths are distributed in a prefixed plane that contains the blade surface and extends to the wake about 1-1/2 chord lengths. At the end of the plane is attached another source line having an unknown polynomial strength that is to be solved along with the double polynomial coefficients by the least squares method. The solution is a function of propeller geometry, given thrust or power, blade load distribution, advance coefficient, and cavitation number.

The induced axial, radial, and tangential velocities--thus pitch and camber distribution--are obtained on a blade-reference surface that allows arbitrary skew, rake, and radial pitch variation. The blade cavity shape is obtained as a correction to the blade cavity derived from supercavitating cascade theory. The thrust and torque coefficients are obtained from the pressure on the blade surface, which is converted from the lift distribution through the Kutta-Joukowsky theorem.

If the hub boundary condition is not considered in solving for the cavity source distribution, the radial velocity caused by the cavity source is not stable. When the hub boundary condition is considered, the numerical results are shown to have reasonable convergence in many numerical experiments. Two new supercavitating propellers were designed using numerical computations derived during the present program, and models were manufactured. Model test results correlate reasonably well with the computed cavity shapes and powering performance.

GEOMETRY OF THE BLADE

The geometry of the blade of a supercavitating propeller is almost the same as that of a subcavitating propeller. The blade is represented in the flow by singularity distributions of vortices and sources on the blade-reference surface in the linear version. Thus, the blade-reference surface has to be known approximately, although the blade shape has to be obtained as a solution. As in the theory for subcavitating propellers, the reference surface will be close to the helical surface of the hydrodynamic pitch angle β_i obtained in the preliminary design. Although the reference surface could be determined more accurately by an iterative procedure, in the present program β_i is used once without iteration, which is considered to be a reasonable approximation. The pitch angle of the reference surface of the wake can be set differently from that of the blade.

A cylindrical coordinate system (x,r,θ), seen in Figure 1, is defined; the x-axis is coincident with the axis of rotation of the propeller and is positive when facing downstream. Thus, the reference surface can be represented by

$$x = \lambda\theta + \zeta(r), \qquad r_H < r < 1, \ \theta_L < \theta < \infty \tag{1}$$

$$\lambda = r \tan \beta_i \tag{2}$$

where $\zeta(r)$ depends on rake and skew, and λ is in general close to a constant. If a Cartesian coordinate is defined as in Figure 1, the parametric representation of the reference surface $\bar{x}(r,\theta) = x\bar{i} + y\bar{j} + z\bar{k}$ is

$$\begin{aligned} x(r,\theta) &= \lambda\theta + \zeta(r) \\ y(r,\theta) &= r \cos\theta \\ z(r,\theta) &= r \sin\theta \end{aligned} \tag{3}$$

Then the area element is

$$dS = \sqrt{EG-F^2}\, dr d\theta \equiv H\, dr d\theta \tag{4}$$

where

$$E = \bar{x}_\theta \cdot \bar{x}_\theta = r^2 \sec^2 \beta_i$$

$$G = \bar{x}_r \cdot \bar{x}_r = (\theta\lambda_r+\zeta_r)^2 + 1 \tag{5}$$

$$F = \bar{x}_r \cdot \bar{x}_\theta = \lambda(\theta\lambda_r+\zeta_r)$$

Thus

$$dS = [\lambda^2+r^2+r^2(\theta\lambda_r+\zeta_r)^2]^{1/2}\, dr d\theta \tag{6}$$

The unit vector normal to the reference surface is

$$\bar{n} = \frac{\bar{x}_\theta \times \bar{x}_r}{|\bar{x}_\theta \times \bar{x}_r|} = \frac{\bar{x}_\theta \times \bar{x}_r}{\sqrt{EG-F^2}} = \frac{(-r\bar{i}+r(\lambda_r\theta+\zeta_r)\bar{j}+\lambda\bar{k}}{H} \tag{7}$$

If λ and ζ are independent of r, the normal vector in Equation (7) is on the cylinder, r = constant. That is, the radial component of the normal vector is zero. Two convenient unit vectors tangential to the reference surface are

$$\frac{\bar{x}_\theta}{|\bar{x}_\theta|} = \frac{\bar{x}_\theta}{\sqrt{E}} \equiv \frac{\bar{x}_\theta}{H_1} \tag{8}$$

and

$$\frac{\bar{x}_r}{|\bar{x}_r|} = \frac{\bar{x}_r}{\sqrt{G}} \tag{9}$$

The curvilinear distance is measured along the helix on the reference surface from the $\theta = 0$ plane to the leading and the trailing edges, denoted by S_ℓ and S_t, respectively. The chord length of the propeller blade at any radius is

$$c(r) = S_t(r) - S_\ell(r) \tag{10}$$

VELOCITIES DUE TO SINGULARITIES

Both a source distribution with strength $m(r,\theta)$ per unit area and a vortex distribution with strength $G(r,\theta)$ per unit area are distributed on each blade-reference surface. Then, the velocity $\bar{u}^m$ caused by the source distribution is derived from potential theory

$$\bar{u}^m(x,r,\theta) = -\frac{1}{4\pi} \int m(\rho,\phi)\, \nabla_x \left(\frac{1}{B}\right) H\, d\rho d\phi \tag{11}$$

The velocity $\bar{u}^G$ caused by the vortex distribution is derived from the Biot-Savart law

$$\bar{u}^G(x,r,\theta) = \frac{1}{4\pi} \int G(\rho,\phi)\, \frac{d\bar{\ell}_x}{B^3}\, \bar{B} \tag{12}$$

where

$$B = \left\{(x-\xi)^2 + r^2 + \rho^2 - 2r\rho\, \cos(\phi+\delta_k-\theta)\right\}^{1/2} \tag{13}$$

$$\delta_k = \frac{2k(k-1)}{Z} \tag{14}$$

$$\bar{B} = \{x-\xi(\rho)\}\bar{i} + \{r-\rho \cos(\phi+\delta_k-\theta)\}\bar{j} - \{\rho \sin(\phi-\delta_k-\theta)\}\bar{k} \tag{15}$$

where Z is the number of blades

$$d\bar{\ell} = \{\tan\delta\bar{i} + \cos(\phi+\delta_k-\theta)\bar{j} + \sin(\phi+\delta_k-\theta)\bar{k}\}d\rho \tag{16}$$

which is a line element along the intersections of the $\theta = \phi$ plane and the reference surface. δ is the angle between $d\bar{\ell}$ and the x = constant plane or $\tan\delta = \partial x/\partial r = \theta\lambda_r + \zeta_r(r)$. The axial, tangential, and radial components, u_a, u_θ, and u_r are written as follows

$$u_a^m(x,r,\theta) = \frac{1}{4\pi}\int_{r_H}^{1}\int_{\theta_L}^{\infty} m(\rho,\phi)\sum_{k=1}^{Z}\frac{1}{B^3}(x-\xi)\,H\,d\phi d\rho$$

$$u_\theta^m(x,r,\theta) = -\frac{1}{4\pi}\int_{r_H}^{1}\int_{\theta_L}^{\infty} m(\rho,\phi)\sum_{k=1}^{Z}\frac{\rho}{B^3}\sin(\phi+\delta_k-\theta)\,H\,d\phi d\rho$$

$$u_r^m(x,r,\theta) = \frac{1}{4\pi}\int_{r_H}^{1}\int_{\theta_L}^{\infty} m(\rho,\phi)\sum_{k=1}^{Z}\frac{1}{B^3}\{r-\rho\cos(\phi+\delta_k-\theta)\}\,H\,d\phi d\rho \tag{17}$$

$$u_a^G(x,r,\theta) = -\frac{1}{4\pi}\int_{r_H}^{1}\int_{\theta_L}^{\theta_T} G(\rho,\phi)\sum_{k=1}^{Z}\frac{1}{B^3}\{r\sin(\phi+\delta_k-\theta)\}\,H\,d\phi d\rho$$

$$+\frac{1}{4\pi}\int_{r_H}^{1}\int_{\theta_L}^{\infty} G_s(\rho,\phi)\sum_{k=1}^{Z}\frac{1}{B^3}\{\rho^2-\rho r\cos(\phi+\delta_k-\theta)\}\,H\,d\phi d\rho \tag{18}$$

(cont.)

$$u_\theta^G(x,r,\theta) = \frac{1}{4\pi}\int_{r_H}^{1}\int_{\theta_L}^{\theta_T} G(\rho,\phi)\sum_{k=1}^{Z}\frac{1}{B^3}\,[\{r\tan\delta-(x-\xi)$$

$$\times\cos(\phi+\delta_k-\theta)\}-\rho\tan\delta\cos(\phi+\delta_k-\theta)]\,H\,d\phi d\rho$$

$$-\frac{1}{4\pi}\int_{r_H}^{1}\int_{\theta_L}^{\infty} G_s(\rho,\phi)\sum_{k=1}^{Z}\frac{\rho}{B^3}\,[\rho\tan\beta_i\cos(\phi+\delta_k-\theta)$$

$$-(x-\xi)\sin(\phi+\delta_k-\theta)-r\tan\beta_i]\,H\,d\phi d\rho \qquad (18)$$

$$u_r^G(x,r,\theta) = \frac{1}{4\pi}\int_{r_H}^{1}\int_{\theta_L}^{\theta_T} G(\rho,\phi)\sum_{k=1}^{Z}\frac{1}{B^3}\,\{(x-\xi)\sin(\phi+\delta_k-\theta)$$

$$+\rho\tan\delta\sin(\phi+\delta_k-\theta)\}\,H\,d\phi d\rho$$

$$+\frac{1}{4\pi}\int_{r_H}^{1}\int_{\theta_L}^{\infty} G_s(\rho,\phi)\sum_{k=1}^{Z}\frac{\rho}{B^3}\,\{\rho\tan\beta_i\sin(\phi+\delta_k-\theta)$$

$$+(x-\xi)\cos(\phi+\delta_k-\theta)\}\,H\,d\phi d\rho$$

where r_H = hub radius

$G_s = -\,dG(\rho,\phi)/d\rho$ = trailing vortex strength in $\theta_L < \phi < \infty$

subscripts a, θ, and r indicate axial, tangential, and radial components, respectively

The induced velocity component due to the singularity distributions, normal and tangential to the blade-reference surface, can then be written in a linear approximation from Equations (5) and (7)

$$u_n = \frac{1}{H(r,\theta)} \left\{ ru_a - \lambda(r) u_\theta - r \left(\theta \frac{d\lambda}{dr} + \frac{d\zeta}{dr} \right) u_r \right\} \tag{19}$$

$$u_r = \frac{1}{H_1(r,\theta)} (\lambda u_a + r u_\theta) \tag{20}$$

where

$$H_1 = r \sec \beta_i \tag{20-1}$$

CAVITY BOUNDARY CONDITION

The cavitation number defined with respect to ship speed V_s is written

$$\sigma = \frac{P_\infty - P_c}{\frac{1}{2} \rho V_s^2} \tag{21}$$

where P_∞ is the pressure infinitely far upstream and P_c is the pressure on the cavity. From the Kutta-Joukowsky theorem the vortex distribution can be written in a nondimensional form (Appendix A) as

$$\frac{G}{V_s} = \frac{1}{2} (p+\sigma) \frac{V_s}{V} \frac{V}{V_\ell} \tag{22}$$

where

$$p = \frac{P - P_\infty}{\frac{1}{2} \rho V_s^2}$$

$$V = (V_a^2 + r^2 \omega^2)^{1/2} \tag{23}$$

P is the pressure on the foil, and V_ℓ is the local velocity. In designing a foil, we can use the local velocity obtained during preliminary design

$$V_\ell = \{(V_a+u_a)^2+(r\omega+u_\theta)^2\}^{1/2} \tag{24}$$

where $V_a = V_s\ (1-w)$

w = wake fraction

ω = angular speed

When the supercavitating propeller, advancing with velocity V_a, is represented by source and vortex distributions, the perturbation velocity component parallel to the blade-reference surface can be written by a linear approximation of the Bernoulli equation of flow, referring to a moving frame of reference (Appendix A), as

$$\frac{u_T^m}{V_s} + \frac{u_T^G}{V_s} = -\frac{p}{2}\frac{V_s}{V} \tag{25}$$

on the pressure side of the blade, and

$$\frac{u_T^m}{V_s} + \frac{u_T^G}{V_s} = \frac{\sigma}{2}\frac{V_s}{V} \tag{26}$$

on the cavity, since

$$\begin{aligned} u_{T+}^G - u_{T-}^G &= G \\ u_{T+}^G + u_{T-}^G &= 2\,u_f \end{aligned} \tag{27}$$

where u_f is the tangential velocity due to the vortex distribution at all points except the point concerned; subscripts "plus" and "minus" indicate the values on the

upper and lower sides of the mean camber of the blade, respectively; from Equations (25) through (27) the tangential velocity due to the source distribution alone can be written as

$$\frac{u_T^m}{V_s} = -\frac{G}{2V_s}\frac{V_\ell}{V} + \frac{\sigma}{2}\frac{V_s}{V} - \frac{u_f}{V_s} \qquad \text{on the blade plane} \quad (28)$$

and

$$\frac{u_T^m}{V_s} = \frac{\sigma}{2}\frac{V_s}{V} - \frac{u_f}{V_s} \qquad \text{on the cavity plane behind the blade} \quad (29)$$

When G and σ are known, these two equations will form a system of Fredholm integral equations of the first kind for the source distribution.

When the propeller blade shape is given instead of the vortex distribution, the problem becomes one of prediction rather than design, and the boundary condition on the pressure side of the blade is

$$\frac{u_n}{V_s} = \frac{dF}{dx} \quad (30)$$

where F is the blade ordinate with respect to the reference surface and $x = \rho\phi \sec \beta_i$.

In this case the blade reference surface must be in close agreement with the mean camber and the wake surfaces. Now Equations (28) through (30) become the integral equations for both sources and vortices. Thus, the prediction problem becomes more complicated. In this report only the design problem is considered. However, the prediction problem can be solved similarly.

SOLUTION FOR SOURCE

For the lifting-surface design of supercavitating propellers, the load distribution $p + \sigma$ on the blade is supplied from the preliminary design computations. As

for subcavitating propellers, the pitch angle β_i of the blade-reference surface is taken as the hydrodynamic advance angle given by the preliminary design calculations. Then, were the source distributions known, all the induced velocities could be computed, and the blade-cavity shape and the final pitch could be obtained in a manner similar to that used for a subcavitating propeller.

Two problems, strength and the location, are related to the source distributions. The location may be considered to be on the blade reference surface. But, how far downstream should the sources be distributed? A two-dimensional supercavitating cascade section could be considered to contribute to the source distribution. When the Riabouchinsky cavity model is used, the cavity source will be confined inside a finite cavity domain. Thus the cavity domain supplied by two-dimensional theory could be used in an attempt to solve the source strength distribution.[12-14] If the linear double spiral vortex model is used, the source distribution does not terminate at the cavity end, but the wake source continues from the end of the cavity. Although there exists a logarithmic singularity in the normal velocity at the cavity end, the streamline represented by the integration of the normal velocity continues smoothly at the cavity end. Any cavity mode is known to give reasonable predictions of lift and drag. Therefore, it may be better to free ourselves from the concept of a finite cavity platform and to consider the cavity wake-source distribution as beginning behind the leading edge. The major question is where to truncate and how to reduce the truncation error.

Even if the problem of the source domain were solved, the method of solution would be far from definite because there is no established method to solve the Fredholm singular integral equation of the first kind; there are suggestions, however, that a series of eigenfunctions could be used.[15] Thus solutions to the three-dimensional problem of a supercavitating foil are complicated and time consuming.

To arrive at a reasonable method to solve the present problem, we considered a combination of three-dimensional corrections to a two-dimensional solution and the series of eigenfunctions. That is, the two-dimensional solution for the supercavitating cascade is multiplied by a double polynomial function with unknown coefficients

$$f(\rho,\phi) = \sum_{i=1}^{J} a_{i1}\,\rho^{i-1} + \sum_{i=1}^{J}\sum_{j=2}^{J} a_{ij}\,\rho^{i-1}\,x^{j-1} \quad \text{in the blade plane} \qquad (31)$$

with $x = H_1\phi$, which is zero at the trailing edge, and

$$f(\rho,\phi) = \sum_{i=1}^{J} a_{i1}\,\rho^{i-1} + \sum_{i=1}^{J}\sum_{j=2}^{J} b_{ij}\,\rho^{i-1}\,x^{i-1} \qquad \text{in the cavity plane} \tag{32}$$

The two-dimensional solution is supplied from preliminary design of each section. The cavity plane has to be finite numerically. A separate source distribution along the truncation line of the cavity is considered with unknown coefficients to compensate for truncation of the cavity:

$$f_2(\rho) = H\Delta\phi \sum_{i=1}^{J} a_i\,\rho^{i-1} \tag{33}$$

In addition, the cavity thickness near the leading edge is specified to be equal to that computed from cascade theory during preliminary design. This thickness is chosen because many sets of cavity thicknesses give the same load distribution and the same cavitation number for the linearized, two-dimensional cavity problem. The leading edge conditions can be interpreted as follows: the source distribution at the leading edge is exactly the same as that of a two-dimensional supercavitating cascade, that is

$$f(\rho,\phi)_{\text{at the leading edge}} = 1 \tag{34}$$

With the previously described representations of the source distribution, the integration of each term in the integral equation is performed numerically. If the propeller blades have rake or skew, ξ is a function of ρ. This is treated by a linear approximation in each $\Delta\rho$ interval

$$\xi = \xi_o + \rho\,\xi_1 \tag{34-1}$$

where

$$\xi_1 = \frac{\partial}{\partial\rho}\,(\lambda\theta+\zeta)_{\rho=\rho_1} = \tan\,\delta$$

$$\xi_o = (\lambda\theta+\zeta)_{\rho=\rho_1} - \rho_1 \tan\,\delta$$

If $\lambda = \rho \tan \beta_i$ is assumed to be a constant in interval $\Delta\rho$, all the integration with respect to ρ can be performed analytically in the interval both on the blade and in the wake.

That is, by substituting Equation (34-1) in B

$$\int \frac{\rho^n}{B^3}\,d\rho \equiv P(n+1)$$

where

$$B = (a\rho^2+2b\rho+c)^{1/2}$$

$$a = 1 + \tan^2\,\delta$$

$$b = -\,\{r\,\cos\,(\phi+\delta_k-\theta) + (x-\xi_o)\,\tan\,\delta\}$$

$$c = r^2 + (x-\xi_o)^2$$

$$P(1) = \frac{1}{ac-b^2}\,\frac{a\rho+b}{B}$$

$$P(2) = \frac{-1}{ac-b^2}\,\frac{b\rho+c}{B}$$

$$P(3) = \frac{1}{a^{3/2}}\,\log\left(\frac{a\rho+b}{\sqrt{a}} + B\right) + \frac{(2b^2-ac)\;\rho+bc}{a(ac-b^2)\;B} \qquad (35)$$

$$P(n+1) = A \frac{\rho^{n-1}}{B} + B_o P(n) + E P(n-1)$$

where

$$A = \frac{1}{(n-2)\ a}$$

$$B_o = -\frac{(2n-3)}{(n-2)} \frac{b}{a}$$

$$E = -\frac{(n-1)\ c}{(n-2)\ a} \qquad n \geq 3$$

The integration with respect to ϕ is performed using the trapezoidal rule. Then the integral equation can be represented as a system of linear, simultaneous equations for the unknown coefficients a_{ij}, b_{ij}, and a_i

$$\sum_{i=1}^{l}\sum_{j=1}^{J} a_{ij}A_{\ell m(ij)} + \sum_{p=1}^{P}\sum_{q=1}^{Q} b_{pq}A_{\ell m(pq)} + \sum_{k=1}^{K} a_k A_{\ell m(k)} = \begin{cases} -\frac{G}{2V_s}\frac{V_\ell}{V} + \frac{\sigma}{2}\frac{V_s}{V} - \frac{u_f}{V_s} \equiv \frac{u_T^m}{V_s} \\ \text{on the blade plane} \\ \frac{\sigma}{2}\frac{V_s}{V} - \frac{u_f}{V_s} \equiv \frac{u_T^m}{V_s} \\ \text{on the cavity plane} \end{cases} \tag{36}$$

where the $A_{\ell m}$ are the integrations of the double integrals of source distribution in Equations (18), (20), (27)-(29) both on the blade and the cavity planes at the ℓth collocation point, and m(ij) is the index corresponding to the coefficient a_{ij}.

By the least-squares method of solving simultaneous equations, a square matrix (B_{pq}) is made out of the generally nonsquare matrix (A_{ij}) where

$$B_{pq} = \sum_{\ell}^{L} A_{\ell p}\ A_{\ell q} \tag{37}$$

and the right side of the matrix is

$$B_p = \sum_{\ell}^{L} C_\ell \, A_{\ell p}$$

where C_ℓ represents the right side of simultaneous Equations (36). The solution of the simultaneous equation

$$\sum a_{ij} \, B_{pq(ij)} + \sum b_{\ell m} \, B_{pq(\ell m)} + \sum a_k \, B_{pq(k)} = B_p \qquad (38)$$
$$p = 1, 2, \ldots.$$

is the desired least squares solution for the cavity source.

IMAGES FOR THE HUB

To satisfy the hub boundary condition

$$u_r = 0 \qquad \text{on } r = r_H$$

the two image systems for vortex and source distributions were considered separately.

The hub images for the vortex distribution are the same as those Kerwin[6] used. That is, the same vortex strength as that distributed on the blade (x,r_1,θ) is used at the image point (x_1,r_2,θ) where $r_1 \cdot r_2 = r_H^2$. Then the trailing vortices tend to cancel the radial velocity on the hub. This is an approximation to a two-dimensional vortex outside a circular cylinder.

The hub images for the source distribution need special consideration because the cavity sources for a supercavitating propeller are much stronger than those of subcavitating propellers. The first approximation of the image source may be taken from an approximation of the hub by a sphere. The image system for a point source of a unit strength at $r = r_1$ of a sphere is a point source at $r_2 = r_H^2/r_1$ with the strength r_H/r_1 and a line sink stretching from $r = r_2$ to the center of the sphere with the strength $1/r_H$. In this way the total absolute strength of the line sink is equal to the point source at $r = r_2$. Thus, on the sphere, $r = r_H$, the normal

velocity induced by the source outside of the sphere is canceled by the image source system; however, outside the sphere, the velocity field due to the image system decays as flow caused by a doublet inside the sphere.

The image source distribution is multiplied by the same double polynomial as Equations (31) and (32), and the hub boundary conditions are considered together with the cavity boundary conditions, Equations (28) and (29), to solve the simultaneous Equations (33), (34), and (36) by the least-squares method. The solution is checked to see if it actually satisfies the hub boundary condition in addition to the cavity boundary conditions.

BLADE SECTION SHAPE

When the unknown coefficients are obtained from Equation (38), the source distribution is computed from Equations (31) and (33). Thus, all the induced velocities can be calculated. It is possible to obtain the section shape of the propeller blade by integrating the velocity field along the blade reference surface. However, this may require a large amount of velocity information. Thus, the method used by Kerwin[6] is followed to correct the foil shape derived from supercavitating cascade theory in the preliminary design process. At a field point of each section the normal velocity component V_{3n} is obtained on the pressure surface of the blade from the lifting-surface theory, and V_{3n} is matched with the corresponding normal velocity obtained from supercavitating cascade theory

$$\sum_{i=o}^{m} a_i \, x^i + c_o \, v_{2n} = v_{3n} \tag{39}$$

where a_i and c_o = unknown coefficients

v_{2n} = normal velocity component on a foil of a supercavitating cascade

x = distance from the leading edge

The unknown coefficients are determined by the least-squares method. That is, the coefficient c_o and the terms $a_i \, x^i$ are the correction to the normal velocity component of the two-dimensional supercavitating cascade caused by the effects of the lifting surface, three-dimensional cavity, flow retardation, etc. For a

subcavitating propeller, an airfoil with the same pressure distribution and the same source distribution has been used[6] instead of a supercavitating cascade. When v_{2n} is represented as the angle of the two-dimensional velocity with respect to the nose-tail line and v_{3n} is represented as the angle of the three-dimensional velocity α with respect to the geometric advance angle β, then by taking a single term in the summation of Equation (39), a_o will be interpreted as the corrected angle of attack of the nose-tail line with respect to β, and c_o will indicate a camber correction of the two-dimensional foil.[6] In the general case the angle of attack will be

$$a_o + \frac{a_1}{2} c + \frac{a_2}{3} c^2 + \ldots \tag{40}$$

and the camber correction due to $\sum a_i x^i$ has to be considered in addition to the correction due to c_o. The optimum number of terms in Equation (39) depends upon the number of collocation terms.

FORCES ON THE BLADE

As in the two-dimensional supercavitating flow, lift and drag should be evaluated by integrating pressure on the blade surface. The section drag in the direction of the nose-tail line is

$$C_D = c \int_o^1 (p+\sigma)\, v_{3n}\, dx + \frac{1}{2} C_{DV} \equiv C_{DC} + \frac{1}{2} C_{DV} \tag{41}$$

since

$$\oint v_{3n}\, dx = 0 \tag{42}$$

where C_{DV} is the friction drag, which is the same as C_D for the subcavitating case.[6] From the Kutta-Joukowsky theorem, Equation (22),

$$p + \sigma = \frac{2G}{V_s} \frac{V_\ell}{V_s}$$

where V_ℓ can now be represented by induced velocities. Thus

$$C_{DC} = \frac{2c}{V_s} \int_o^1 V_\ell \frac{G}{V_s} v_{3n} \, dx \tag{43}$$

By writing

$$\frac{V_\ell}{V_s} = \sum_{k=1}^{L} c_k \, x^{k-1}$$

$$C_{DC} = 4\pi\Gamma \int_o^1 \sum c_k \, x^{k-1} \, \gamma \left(\sum a_i x^i + c_o v_{2n} \right) dx$$

$$= 4\pi\Gamma \int_o^1 \left(\sum_i \sum_{k=1}^{L} c_k a_i x^{k+i-1} + c_o \sum_{k=1}^{L} c_k x^{k-1} v_{2n} \right) \gamma \, dx$$

where

$$\Gamma\gamma c = \frac{G}{2\pi V_s} \text{ and } \int_o^1 \gamma \, dx = 1$$

Likewise the sectional lift ccefficient can be written

$$C_L = c \int_o^1 (p+\sigma) \, dx = \frac{2c}{V_s} \int_o^1 V_\ell \frac{G}{V_s} \, dx$$

$$= 4\pi\Gamma \int_o^1 \sum_k c_k \, x^{k-1} \, \gamma \, dx \equiv 4\pi\Gamma \sum_k c_k \, P_k \tag{44}$$

Since v_{2n} and γ are available from the preliminary design calculations

$$P_k = \int_o^1 x^{k-1} \gamma \, dx$$

and

$$Q_k = \int_o^1 x^{k-1} v_{2n} \gamma \, dx$$

can also be precalculated in the preliminary design. Then the nondimensional thrust and power coefficients are obtained in a conventional way:[6]

$$C_T \equiv \frac{T}{\frac{\pi}{2} \rho V_s^2 R^2} = \frac{Z}{\pi} \int_{r_H}^1 (C_L \cos \phi - C_D \sin \phi) \, dr$$

$$C_P \equiv \frac{\omega Q}{\frac{\pi}{2} \rho R^2 V_s^3} = \frac{Z}{\pi\lambda} \int_{r_H}^1 r(C_L \sin \phi + C_D \cos \phi) \, dr \qquad (45)$$

where T = propeller thrust

Q = propeller torque

ϕ = pitch angle, i.e.,

$$\phi = \beta + \alpha$$

The efficiency of the propeller is given by

$$\eta = \frac{C_r}{C_p}$$

NOTE ON PRELIMINARY DESIGN PROGRAM

As for subcavitating propellers, the preliminary design calculations form a separate program;[11] however, it is necessary to briefly explain this subject to help understand the final design procedures.

The present preliminary design of a supercavitating propeller is more or less a combination of subcavitating lifting-line theory and two-dimensional supercavitating cascade theory.[16] The cavity drag-lift ratio will be iteratively fed from the latter into the former so as to compute the circulation and pitch of the blades needed to produce a given thrust. In addition, the foil shape is determined so that the drag-lift ratio is not too large for a reasonably thick cavity. Both the cavity thickness near the leading edge, and the minimum cavity length must be prescribed because supercavitating propellers are supposed to have a clean cavity covering the suction side of the blade. However, this cavity length is a function of not only foil shape but also the cavitation number, which is determined by the design conditions. To design such a foil, it is convenient to consider three elementary foils: a basic, cambered low-drag foil, such as the two-term camber foil; a flat plate to supply angle of attack; and the leading-edge singularity to supply the leading-edge cavity thickness. Called a point drag[16] because it produces no lift, the leading-edge singularity is especially useful for creating a long cavity. This is so because the infinite cavity cavitation number of a supercavitating cascade is linearly proportional to leading-edge thickness;[16] see Figure 2. Figure 2 shows the relationship between cavitation number and leading-edge thickness for a supercavitating propeller.[16] Model 3770 in Figure 2 will be used for the numerical test and is discussed in more detail later.

In general, the specification for the leading-edge cavity thickness is based upon the strength requirement. When the cavitation number is relatively large, however, the leading-edge cavity thickness may have to be greater than the strength condition requires. This greater thickness is needed to allow cavity lengths that are more than 50 percent longer than the chord. Each section has different cascade parameters, i.e., the solidity and the stagger angle;[16] see Figure 3. The present preliminary design method allows the option of using either a specified basic load distribution or a specified basic camber shape for the blade section. In an actual design, the given basic camber shape of the blade section seems to be more convenient. Given the basic camber shape (the two-term camber in an infinite medium

normalized by the lift coefficient, for example) one finds the shock-free angle at each station of a supercavitating propeller blade by considering a supercavitating cascade of infinite cavity length at each blade section. The angle of attack and the point drag are combined with the basic shock-free camber to supply the given leading-edge thickness, the minimum cavity length, and the required load distribution. In this process there are two options: either the camber or the angle of attack per unit lift coefficient is preset,[11] where the former is Case 1 and the latter is Case 2.

The hydrodynamic advance angle β_i can be determined by either of two ways: any form of tan β_i may be preset, such as tan $\beta_i = c/r$, or the optimum pitch condition for the supercavitating propeller[17] may be preset

$$\frac{r}{\lambda} \tan \beta_i = \left| c(1-t) - \left(\varepsilon + G \frac{d\varepsilon}{dG}\right) \frac{r}{\lambda} \right|^{1/2} (1-w)^{1/2} \left| 1 + c(1-t) - \left(\varepsilon + G \frac{d\varepsilon}{dG}\right) \frac{\lambda}{r} \right|^{-1/2} \quad (46)$$

where ε is the drag-lift ratio, and t is the thrust deduction.

Since the local cavitation number is fixed according to the design conditions, and the lift coefficient varies for each iteration, the cavity length may also vary. Therefore, the sectional supercavitating cascade problem must be solved for each section and for each iteration. This requires a great deal of computer time. We resolved this difficulty by conveniently treating the cavity problem as a foil having infinite cavity length with a correction for the finite cavity effect.[16] The former needs to be calculated only once at each blade section, regardless of the number of iterations. Only the finite cavity effect is computed for each iteration, assuming the same load distribution as for infinite cavity length. Thus, the finite cavity effect appears as a reduction of angle of attack and camber.

The output of the preliminary design program consists of the thrust and power coefficients, circulation and lift distribution, tan β_i, pitch distribution, efficiency, etc. Normal velocity distribution on the cavity and foil, foil cavity shape, load distribution, and other necessary data are stored on a tape to be fed into the lifting-surface design.

NUMERICAL SCHEMES AND COMPUTER PROGRAM

There are several computer programs for lifting-surface design of subcavitating propellers. Supercavitating propellers are similar to wide- and thick-bladed subcavitating propellers when the cavity thickness is known; therefore, it would seem reasonable to use an existing computer program for subcavitating propellers rather than to start the entire complicated program from scratch. Among the available programs, the recent program by Kerwin was chosen for two reasons: (1) it included the effect of sources and vortices, and (2) it could include the effects of rake and skew with variable λ.

The main differences between the programs for supercavitating and subcavitating propellers are as follows. The strengths of source distributions are not known in the supercavitating case because the cavity shape is not known while the blade thickness is assumed to be known for the subcavitating case. Therefore, the program for solving the cavity-source distribution is written according to the present theory explained in the previous section and becomes the main frame of the present program. Routines in the Kerwin program are used as much as possible. The source is distributed not only on the blade but also in the cavity wake according to Equations (31) and (34). Therefore, the number of meshes for supercavitating propellers is almost as much as two and a half times the number for the subcavitating case. The chordwise load distribution is taken from the supercavitating cascade theory of preliminary design rather than from airfoil theory. The forces on the blade are obtained from Equations (41) and (45).

Figure 4 gives the outline of the flow charts of the lifting-surface program.

Attention should also be drawn to the following points, which differ from the existing program for subcavitating propellers.

Because of the singular behavior of the kernels of integrals appearing in the induced velocity expressions in Equations (17) and (18), all the integrations related to bound and trailing vorticity, and the source distribution are integrated analytically in a small interval of the radial direction on the blade and cavity where the collocation points are located; using Equation (35).

Because of the singularity along the leading edge, both for source and load distribution, the interval that includes the leading edge is treated separately. That is, the leading-edge load is the integrated load obtained when the remaining load distribution is subtracted from the total load. The leading-edge source

strength is represented by the normal velocities of two-dimensional cascade results solved in the preliminary design program; see Appendix B.

For convenience, short cavity effects of the supercavitating cascade are computed in the lifting-surface theory, when the two-dimensional cascade is used as an approximate solution to be corrected.

After computing all the B_{pq} coefficients of Equation (37), the simultaneous Equations (38) are solved by a subroutine which uses a Gaussian elimination method. The accuracy of the solution obtained by the least-squares method is approximately checked by a comparison of the left-hand and right-hand sides of Equation (28). Then the total source strength on the blade is obtained from Equation (31). The velocity component due to sources is obtained from all the velocity component functions created for A_{pq} in Equation (36).

Because many existing supercavitating-propeller models have chord lengths smaller near the blade tip than near the hub, angular intervals near the tip are too small. Thus, the present program allows intervals of all the even degrees, such as 2, 4, etc. In addition, a 1-deg interval is tested for a six-bladed propeller. This feature is supplied by using the addition rule of trigonometry, making use of data stored for cosine and sine functions.

When the rake and skew are present in the reference surface, the correct area element $Hd\rho d\phi$ in all the area integrals has to be taken into account instead of $H_1 d\rho d\phi$.

The collocation points can be taken to be 10 points on the blade and 5 points on the cavity wake. However, if four points are selected on the blade this will be exactly the same as the collocation points for the subcavitating case, except for the extra points on the cavity wake.

In addition to other preliminary data, the P_n and Q_n in Equation (44) are prepared in the preliminary design and are conveyed through an input tape. As in the subcavitating case, friction is taken into account, but only on the pressure side.

The output routine is created in a format similar to that of Kerwin by considering data taken from the supercavitating cascade of the preliminary design for the blade-section and the cavity shapes.

The input to the computer program includes the same information as is used for the subcavitating propeller design, such as rpm; ship speed; propeller diameter; hub diameter; helical distance from an arbitrarily fixed reference plane, distance from

the x-y plane to the leading and trailing edges of the blade; inflow velocity ratio V_A/V_S; number of collocation points on the blade, cavity wake, etc. Also, as mentioned previously, the data tape created by the preliminary design program for all the necessary sectional data from the supercavitating cascade theory is fed into the lifting-surface design.

The output consists of the components of induced velocities resulting from the vortex and source distributions, correction factors for source strength and camber, angle of attack relative to β, pitch distribution, thrust and torque coefficients, and efficiency.

NUMERICAL EXPERIMENTS FOR SOLUTION

The cavity model, the solution for cavity source strength, the number of intervals for vortex and source distributions, the number of collocation points, and the like cannot be determined theoretically; instead, they must be determined according to the behavior of numerical output. The output, especially, should show convergence, which could be built into the program, if the program is simple and does not require too much time. However, a large program, such as the present one, which requires considerable computer time, cannot be run for all values of parameters so as to check convergence of the solution for each design. Instead, it may be enough to check several aspects of parametric changes for a typical case and to assume that the other cases will reasonably follow the typical case.

In the present work, designing the Model 4717 supercavitating propeller, various convergence checks have been performed, and the results will be shown in the follow-up. The design conditions for Model 4717C are shown in Table 1.

The cavity truncation locations were varied from 1.5 to 2.8 chord lengths to check the cavity model. Figures 5 and 6 show that the truncation at 2.2 chord lengths and at 2.5 chord lengths produces almost the same pitch and camber distributions (differing less than 1%); the pitch distribution is about 3% larger than at 1.8 chord lengths.

The influence of the choice of angular interval on pitch and camber distribution is also shown in Figures 5 and 6. By changing 2-deg intervals to 1-deg intervals, the camber correction factor c_o increased about 6% and the pitch diameter ratio P/D increased about 1%. Since the magnitude of camber is so small, a change in the correction factor of 10% is within the manufacturing error. If the blade tip

has more than five intervals, 2-deg intervals are sufficient; finer intervals, which increase costs significantly, appear to be unnecessary.

To check whether there were enough collocation points, we chose 10 points and created the foil shape by plotting streamlines. The results have been compared with the case of four collocation points given in Figures 7 and 8. The simple approximation obtained using Equation (39) is shown to express amazingly close agreement with the plotted streamlines.

In Equation (28) V_ℓ is the local mean speed, which is not known without examination, so the value from the lifting line theory has been substituted for it. However, a more accurate formulation would be Equation (53) (Appendix A) instead of Equation (28).

$$\frac{u_T^m}{V_s} = \frac{1}{\left(2+\frac{G}{V_s}\frac{V_s}{V}\right)}\left\{-\frac{G}{V_s}\left(1+\frac{u_f}{V}\right)-2\frac{u_f}{V_s}+\sigma\frac{V_s}{V}\right\} \tag{47}$$

The computer results for these two cases were almost the same. The present program used Equation (47), although slightly more computer time was needed. When G/V_s is quite large, it may improve the solution.

To check whether the solution satisfies the boundary conditions well, the left-hand and right-hand sides of Equation (47) were plotted in Figures 9-12; and the radial components of velocities on the blades were plotted, Figures 13 and 14. These calculations were made with and without the hub boundary conditions being satisfied when the degrees of ρ and x in the double polynomials in Equations (31) through (33) were taken as 3 in one case and as 5 in the other case. During this process, we noticed an interesting phenomenon: an instability occurred in the numerical value of radial velocity for the solution which did not satisfy the hub boundary condition. That is, if the hub boundary condition was not specified, a slight change of parameters, such as cavity length, number of intervals, or the degree of polynomials, produced large changes in radial velocities. Yet, the numerical values of the thrust and torque coefficients or the pitch distribution did not change too much. This may be because the linear boundary conditions on a cavity or foil do not include any constraint on the radial velocity. In the present problem, the only constraint on

the radial velocity is on the hub condition. Thus, the hub boundary condition is needed not only to find the hub effect on the pitch distribution but also to make the solution stable.

The specified boundary conditions are well satisfied in general, although when the boundary condition on the hub is included, the cavity conditions are slightly less accurate, as shown in Figures 11 and 12. The differences in the radial velocities occurring for the case with and the case without the hub boundary condition (see Figures 13 and 14) indicate an instability. The radial velocity satisfying the hub boundary condition in Figure 13 is the stable solution. In Figure 15 the pitch-diameter ratio is shown for Model 4717C with hub images. In Figure 16 the camber correction factors are shown for Model 4717C with and without hub images. When the computed results obtained without consideration of the hub boundary condition happened to have radial velocities with small values, the results were very close to the solutions obtained when the hub boundary condition was considered. The numerical results reported in the following discussion were obtained without satisfying the hub boundary condition. In the cases given, the instability phenomenon was not noticed.

NUMERICAL EXAMPLES FOR PROPELLER DESIGN AND DISCUSSIONS

Many supercavitating propellers have been designed and tested in the past; of that number, two propellers, DTNSRDC Models 3770 and 3870 were chosen[2] to determine if this design program is reasonable. The former propeller has three blades and a low advance coefficient, and the latter has four blades and a high advance coefficient. Experiments showed that both propellers had smooth cavities. The experimental results and the previous design calculations are available.[2]

The design and performance characteristics of the two propellers are shown in Table 2.

It is extremely difficult to compare the present numerical results to the experimental results for propellers that were designed using an entirely different method. The present program is intended for design, not prediction. The present program does not produce data on leading-edge cavity thicknesses, input that is essential to the design of propellers similar to Models 3770 and 3870. To check the reasonableness of the present program we guessed at the leading-edge cavity thicknesses for Models 3770 and 3870; this is presented in Figure 17. Because the

actual cavity thickness was never measured, this is not a scientific estimate. The leading-edge cavity thickness selected for Model 3770 results in an almost infinite cavity length at every section of the blade, except near the tip and the hub. However, because the design cavitation number of Model 3870 is not very small, the selected leading-edge cavity thickness is not large enough to induce a smooth sheet cavity all over the blade. Therefore, the leading-edge cavity thickness of Model 3870 was corrected to give a cavity length at least 50 percent longer than the chord. To do this, an extra leading-edge point drag was added to the cascade theory used in the present design method, as explained previously. The design thrusts used in the present lifting-line computations are the experimental values listed in Table 2, where Case 1 is for cases without angle of attack and Case 2, with preset angle of attack. It is seen that the efficiencies of the propellers, as predicted by the present method, are very close to the measured efficiencies, even in the preliminary design stage of calculations.

Pitch distributions obtained from the preliminary design and lifting-surface design computations, according to the two design approaches, Case 1 (without angle of attack) and Case 2 (with angle of attack) are shown in Figures 18 through 21 together with the pitches of the two propeller models. The pitch values obtained from the preliminary design calculations are higher than those obtained from lifting-surface calculations because, in preliminary design, the effect of flow retardation is not considered. The pitch distribution is also related to the leading-edge cavity thickness. In general, when the leading-edge thickness increases, the pitch also increases; however, the efficiency decreases slightly. The pitch distributions for the predictions and for the models are noticeably different. This is because the optimum lift distribution and pitch angle, which are influenced by the blade-cavity interference in the present method are quite different from those of the models. If these factors are taken into account, all results appear reasonable compared with those of the models.

The lifting-surface corrections to the source distribution for the two propellers are shown in Figure 22. Although the correction for Model 3770 is close to 1, it is about 20 percent greater near the trailing edge than at the leading edge for Model 3870. If the correction factor is unity, this means that the cascade source strength is the same as the blade cavity source strength. This source strength has

the main influence on pitch, thrust, and efficiency. The calculated efficiency is close to that obtained in the model experiments, as shown in Table 2.

The lifting-surface camber correction factors for the two propellers are shown in Figures 23 and 24. The camber correction factor for Model 3870 is much larger than for Model 3770, as in the calculation of Venning and Haberman.[2] The pitch distribution and camber correction curves for Model 3870 are quite different from those for Model 3770. The former has shorter cavities with four blades and large expanded area ratio (EAR), and the latter has longer cavities with three blades and smaller EAR.

EXPERIMENTAL EVALUATION OF THEORY

Finally, the Center conducted an experimental program to evaluate the present method for designing supercavitating propellers. Two supercavitating propellers were designed, using the present method,[18] for a 200-ton (181 metric ton) hydrofoil craft. The propeller design criteria are given in Table 3. The propeller design characteristics are given in Table 2.

Two model propellers were manufactured from these designs. The geometry of these propellers is given in Table 4 and drawings of the propellers are shown in Figures 25 and 26.

The experimental program was divided into two phases. The results of the first phase, the measurements of blade-cavity shapes, are reported in the following section, while the results of model propeller performance are described in the last section.

EXPERIMENTAL INVESTIGATION OF BLADE-CAVITY THICKNESS DISTRIBUTION

A series of experiments was performed to determine how well linear theory predicted the upper cavity surface location for Propellers 4717C and 4738A. For these experiments, brass pins of varying lengths were attached to the backs of the propeller blades. During propeller operation in the 36-in. variable-pressure water tunnel, one could see when the pins came into contact with the upper cavity surface.

This experimental procedure has already been used to verify the upper cavity surface location for Propeller 4699,[19,20] and the parent design of Propellers 4738A

and 4717C. In addition, cavity heights have been measured in similar ways for a supercavitating flat plate and a Tulin-two-term section by Christopher and Johnson.[21]

DESCRIPTION AND LOCATION OF PINS

Number-four brass machine screws with heads cut off were used as pins. These pins were attached to the blade backs by drilling and tapping holes perpendicular to the surface at 12 locations. The upper cavity surface location was defined as a point on a line, perpendicular to the nose tail line, that runs through the center of the tapped hole at the blade surface; see Figure 27. The holes were drilled and tapped perpendicular to the back of the blade to cant the pins slightly away from the reference line (the line perpendicular to the nose tail line). A slight error was introduced, but the machining process was greatly simplified. The locations of these pins were as follows: 10, 30, 60, and 90 percent of chord at nondimensional radii (r/R) of 0.361, 0.544, and 0.726; see Figure 28. Since the blade at 10 percent of chord was too thin to tap, the pins at these locations were soldered in place. The pins at all other locations were screwed in and secured by tiny electrical lock nuts (see photos in Reference 19).

Three sets of pins were used for testing Propeller 4717C. When installed, the first set of pins protruded above the back of the blades to a height that corresponded to three times the distance from the back of the blades to the theoretically predicted upper cavity surface. The second set of pins protruded by a factor of 1.67 and the third set by a factor of 1.0, the latter being the theoretically predicted cavity height. However, the pins at 10 percent of chord varied from this order; their heights corresponded to cavity-height factors of 3, 2.33, and 1.0. The pins at the 10 percent of chord locations had to be filed by hand to the correct height, and the factor of 2.33 rather than 1.67 was used to ensure that the pin-height would exceed the experimental cavity thickness. The experiments have shown, however, that the theory overpredicted the cavity height near the leading edge, and the pins could have been filed to a height corresponding to a factor of 1.67.

Four sets of pins were used for Propeller 4738A. The first set of pins protruded above the back of the blade to a height corresponding to a factor of 1.8 times the distance from the back of the blade to the theoretically predicted cavity surface. The other three sets corresponded to factor of 1.4, 1.0 (theoretical) and

0.6. The pins at the 10 percent of chord locations were filed to a height corresponding to the multiplication factor used for the other pins in the set being tested.

A thin coat of international yellow paint was applied to the tips of the pins prior to testing to aid in visual observation. The experimenters could thus locate the pins easily when the propeller was revolving.

EXPERIMENTAL PROCEDURE

The propeller rpm was increased until the cavity enclosed all the pins. This procedure was begun with the set of brass pins that protruded highest. While the pressure and velocity in the 36-in. variable pressure water tunnel was held constant, corresponding to the design cavitation number, $\sigma = 0.34$, the propeller rpm was gradually reduced in decrements of 10. Each time the propeller rpm was reduced, a hand-held strobe unit was used to observe visually whether the pins were in or out of the cavity. These observations could be made rapidly, although the pins that barely touched the upper cavity surface required more attention than did the others. When all pins protruded through the cavity surface, the procedure was repeated with another set of pins. A depth micrometer was used before and after each test to measure the height of the pins above the back of each blade. This was done to ensure that the pins were at the correct height and had not moved during testing.

As the pins began to break through the cavity surface, a furrow or small groove formed in the surface, accompanied by some spray or cavitation behind the pin. A directional strobe unit with variable light intensity made these furrows much more visible. This phenomenon has been recorded in several color photographs.[19]

Large, international-yellow numbers painted on the backs of the blades proved invaluable during testing. Also, each propeller hub was coded with a series of dots, the number of which corresponded to the number on each blade.

DISCUSSION OF EXPERIMENTAL RESULTS

Figures 29-31 compare linear theory predictions of cavity height with experimental results for Propeller 4717C. These figures show three experimental upper cavity surfaces corresponding to three values of J, one of which is the design J (1.037). Note that the following relationship gives the advance angle, β, at each radial blade section,

$$\beta = \tan^{-1} (V_A/2\pi rn)$$

$$= \tan^{-1} [J/(\pi r/R)]$$

From this relationship, one can determine, approximately, the corresponding shifts in upper cavity surface that result from small changes in angle of attack. For example, in Figure 29, at the design J (1.037), β is determined to be 42.44 deg. For a J value of 1.0, β = 41.40 deg. Therefore, a change of J corresponding to 0.037 has caused, approximately, a one-deg change in angle of attack, which shifts the cavity surface upwards as shown.

Theoretically, the section lift and cavity thickness for Propeller 4717C are generated entirely by camber and point drag (note the blunt nose in Figures 29 through 31). That is, no incidence was used in the design to generate lift or cavity thickness. In Figures 29 though 31, the theoretical prediction of cavity height agrees fairly well with the experimental data. Near the leading edge, however, the theory appears to overpredict cavity thickness. Also, visual observations indicated that the backs of the blades at all radial sections on Propeller 4717C were wetted to about 2- or 3-percent of chord from the leading edge. At this point, separation was caused by a locally flat area that was inadvertently machined onto the back of the blade. Although this local flat was almost microscopic, it effectively caused separation. Apparently, very near the leading edge some portion of the blade metal was interfering with the upper cavity streamline.

Figures 32 to 34 compare linear theory predictions of cavity height with experimental results for Propeller 4738A. Note in these figures the large amount of point drag or blunt nose indicated by the theory. This results because both Models 4738A and 4717C were designed to have approximately the same full-scale stress levels. This dictated that the maximum, theoretical, cavity thicknesses for Models 4738A and 4717C would be almost the same.[22] To obtain the same maximum thickness in a shorter distance, we used a large amount of point drag together with incidence and camber to generate the theoretical cavity.

Figures 32 to 34 show three experimental upper cavity surfaces corresponding to three values of J. Note that at r/R = 0.361, Figure 32, the blade was fully wetted at the design value of J (1.037); therefore, cavity heights for three other values

of J have been shown. At a J value of 0.98, the experimental cavity surface coincides with the predicted cavity surface height at aft locations on the blade. This J value represents an approximate increase in angle of attack of 1.6 deg over the design value of J. For the cavity surface, corresponding to a J value of 0.96, the increased incidence is equal to about 2.2 deg. However, as mentioned before, the cavity did not spring from the leading edge. It moved down the span as rpm was increased. Since the water-tunnel velocity was held close to 35 fps (10.688 m/sec) and since the model propeller diameter was 16 in. (40.64 cm), the difference in model rpm corresponding to the J values of 0.98 and 1.037 was 88. This corresponds to an increase of about 58 in full-scale rpm. It is also interesting to note that, according to performance evaluation experiments, an increase of 29 rpm, over the 1000 rpm of full-scale design would give the design thrust.

At the two outer radial positions, r/R = 0.544 and 0.726, full cavitation did occur at the design J (1.037), but the theory overpredicted the cavity surface height. As with Propeller 4717C, the back of the blade near the leading edge of Propeller 4738A was wetted to about 2- or 3-percent of chord.

To understand more fully the discrepancy between theory and experiment, the reader should recall that a point drag is a linear theoretical model of the leading edge cavity thickness represented by a point singularity. Experimental results indicate that the actual separation point at the leading edge must be carefully chosen, for example, as a slope discontinuity of the blade surface, to achieve the designed leading edge cavity thickness; if the predicted leading edge cavity, not just 70 percent of it, had been filled by a material up to 2 percent of chord from the leading edge, the experimental results would have almost coincided with the theory, except very near the hub, where the hub effect is important.

CAVITATION PERFORMANCE CHARACTERISTICS OF SUPERCAVITATING PROPELLERS 4717B, 4717C AND 4738A

BACKGROUND

Propeller 4717C was originally manufactured as Propeller 4717B. Propeller 4717B was identical to Propeller 4717C except for the backs of the blades, which had a shape to conform to the predicted cavity shape at design operating conditions. The primary purpose of Propeller 4717B was to determine, by observation, how well the

blade section shape represented the blade cavity shape. Following characterization and observation, Propeller 4717B was finish cut to the final design version, Propeller 4717C.

Propeller 4738A is a six bladed propeller with the same expanded area as the previous four bladed propeller, and is designed for the same conditions as the other propellers.

EXPERIMENTAL PROCEDURE

Cavitation performance characteristics and cavitation observations were obtained in the 36-in. variable pressure water tunnel. Tunnel water velocities were measured by the tunnel venturi system. The scope of the experiments is given in Table 5.

Tunnel pressure and water velocity were set to establish each cavitation number and then propeller revolution rate was varied to cover a range of advance coefficients. Propeller thrust and torque were measured at each condition and sketches were made of the cavitation present. The Reynolds number, R_n, during the experiments ranged from 7.5×10^5 to 5.6×10^6.

PRESENTATION OF DATA AND DISCUSSION

The thrust and torque data were reduced to nondimensional coefficients of K_T and K_Q. Propeller efficiencies were calculated from faired values of K_T and K_Q. The cavitation performance characteristics of the three propellers are presented in Tables 6 through 8.

Curves representing the faired data, from Tables 6 through 8, are shown as an example in Figure 35. Curves of maximum-speed thrust loading (K_T/J^2) have been added to the performance curves for Propeller 4738A. The intersection of the K_TJ^2 curve and the K_T curves at the design sigma (σ) determines the predicted operational point for each propeller. A comparison between the design operational points and the points predicted by the experimental data is given in Table 9.

Sketches of the back cavitation present on the propellers at two cavitation numbers are given in Figures 36 through 38. These sketches cover a range of advance coefficients from partially cavitating to fully cavitating conditions. If advance coefficients had lower values than those shown, the propellers, at the same cavitation number, would also be fully cavitating. With only one exception, propellers

contained no face cavitation over the range of cavitation numbers and advance coefficients covered. The sole exception was at an advance coefficient of 1.2, where some leading edge face cavitation was observed at cavitation numbers of 0.75 and lower.

CONCLUSIONS

At design speed coefficient and design σ, Propeller 4717B contains practically no back cavitation. If advance coefficient is reduced slightly, at design σ, the backs of the blades are covered by sheet cavitation from the blade tip to 50 percent radius. This indicates that the predicted cavity shape over this part of the propeller blades is quite accurate.

Neither of the designed propellers, 4717C and 4738A, had face cavitation at the design operational points. Propeller 4717C essentially had full back cavitation and Propeller 4738A had back cavitation from about 35 percent radius to the tip of the blades at the design operational point.

The propeller theory slightly overpredicted the available thrust for both propellers. Propeller 4717C would require 6 percent more rpm and 8 percent more power than predicted to reach design speed. Propeller 4738A would require 5 percent more rpm but 4 percent less power than predicted to reach design speed. If the operating point is defined as the speed and rpm where the propellers absorb the available maximum power, Propeller 4717C would operate at V_A = 58.7 knots and rpm = 1016, and Propeller 4738A would operate at V_A = 61 knots and rpm = 1054. The propeller efficiencies at these conditions are 66 percent and 67 percent, respectively.

It has been recognized[23] that the nonlinear effects on lift and drag of cavitating foils are approximately equal to $-0.5\ C_L^2/(1+\sigma)$ and $-0.5\ C_D C_L/(1+\sigma)$. Therefore, propellers designed according to the linear theory would produce less thrust, as indicated in the experimental results. However, the leading edge cavity thickness was slightly smaller than the design thickness due to the unmatched separation point and 70 percent filling of cavity thickness. Thus the drag should have been a little less than predicted by the linear theory, as was found experimentally for Propeller 4738A. Because of the decreased efficiency of Propeller 4717C, however, more care may be required in calculating the cavity drag due to the blunt leading edge.

All in all, the design theory predicted the cavity thickness and the propeller performance quite well at the design point, within the bounds of error to be

expected of linear theory. It should be remembered that the present design theory does not include semiempirical formulae or factors. In addition, this verifies that the point drag of linear theory is very useful in solving one of the important problems relating to supercavitating propellers--how to make propeller blades having sufficiently thick leading edges without paying too much of an efficiency penalty.

ACKNOWLEDGMENTS

The authors express their gratitude to Dr. William B. Morgan, Mr. Gabor F. Dobay, and Mr. Edmond R. Caster who managed the overall project and provided much encouragement. The authors would also like to thank the staff at the DTNSRDC 36-inch Water Tunnel Facility for their cooperation during the propeller experiments.

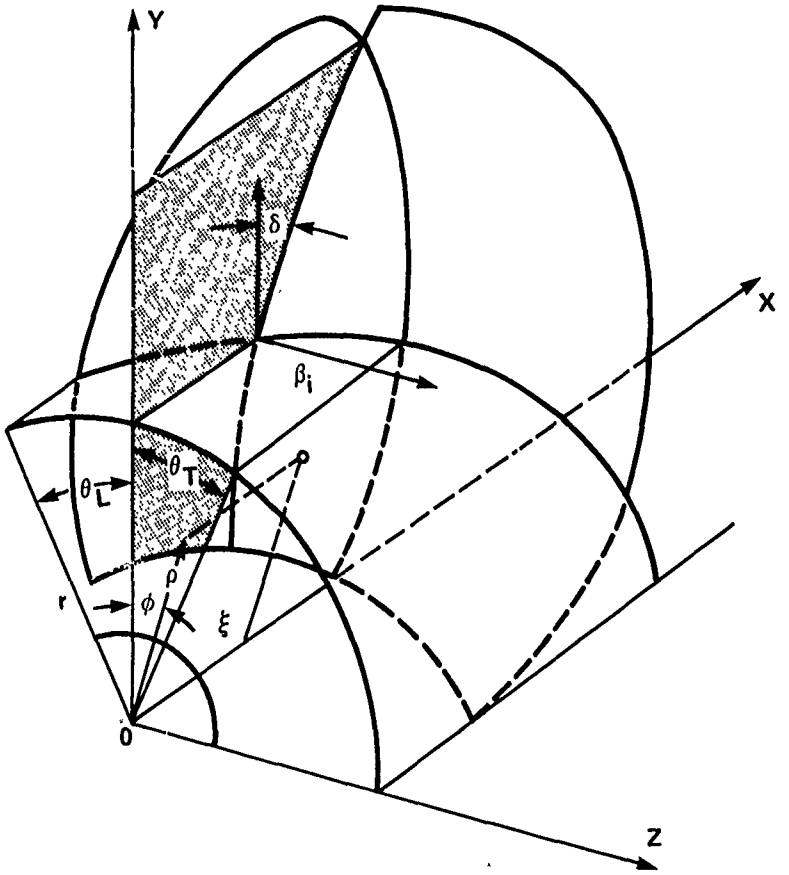

Figure 1 - Coordinate Systems for Blade Surface Reference

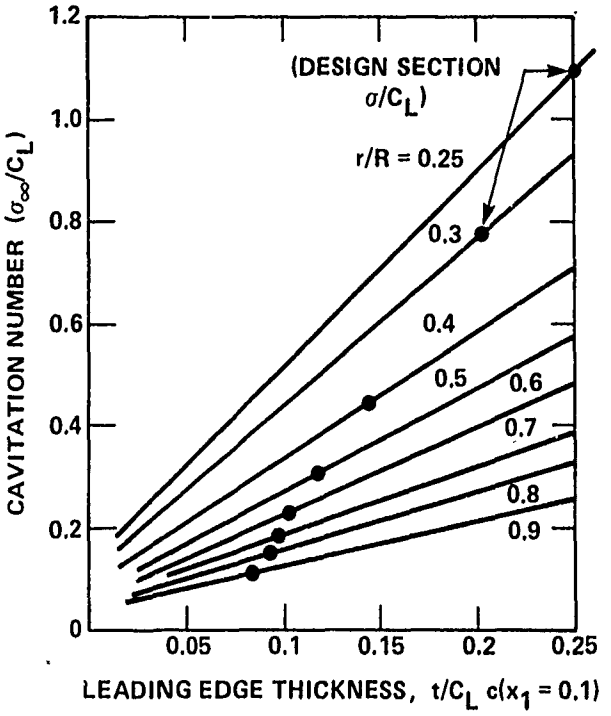

Figure 2 - Example of Relation Between Choked Flow Cavitation Number and Leading-Edge Thickness of Supercavitating Cascade for Blade Sections of Supercavitating Propeller Model 3770

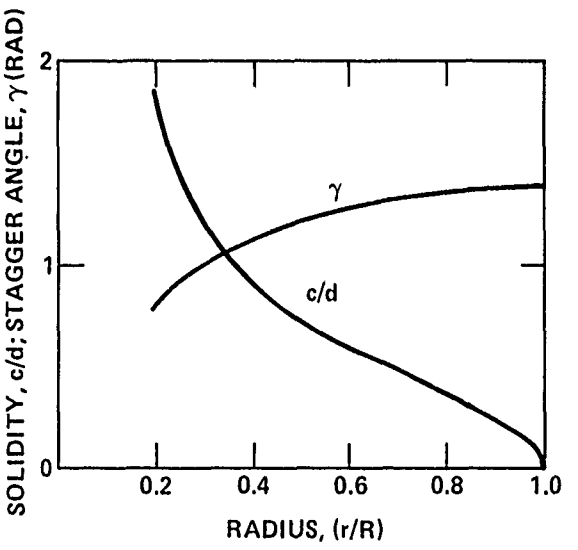

Figure 3 - Example of Cascade Parameters for Supercavitating Propeller Model 3770

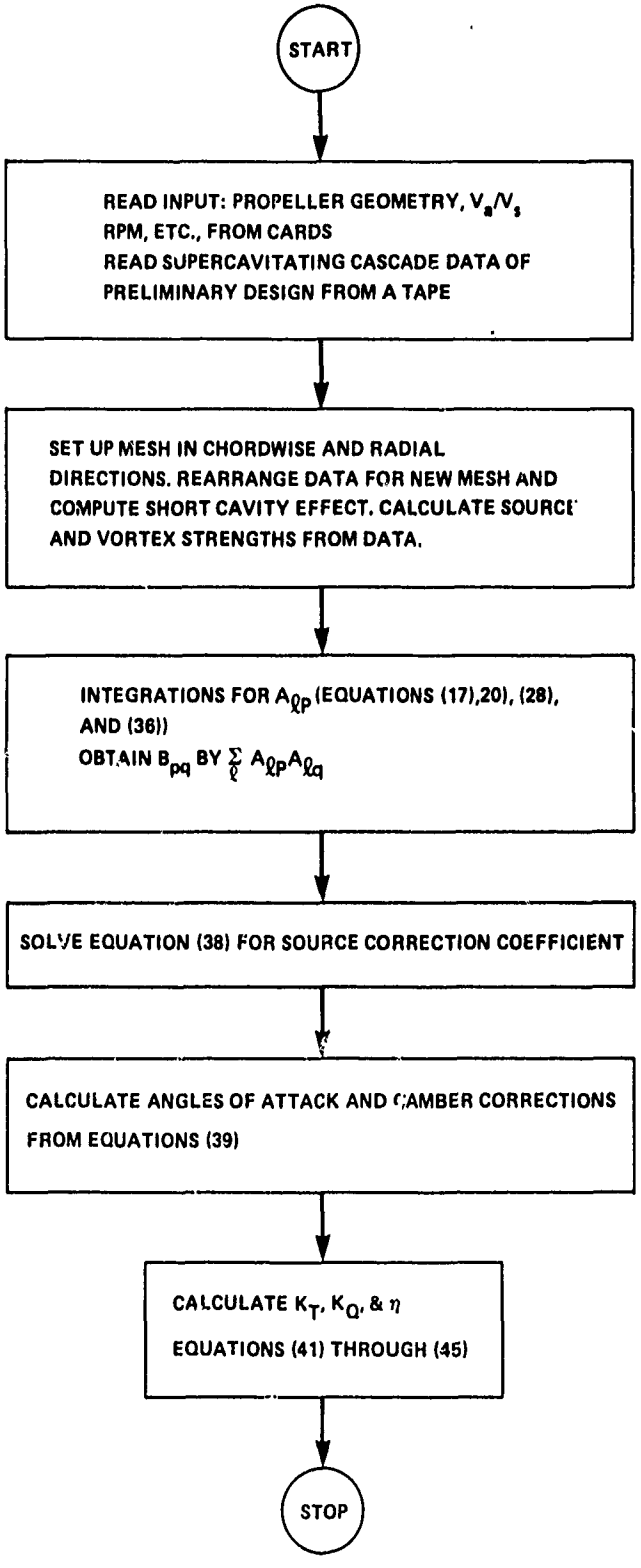

Figure 4 - Flow Chart for Lifting-Surface Design of Supercavitating Propellers

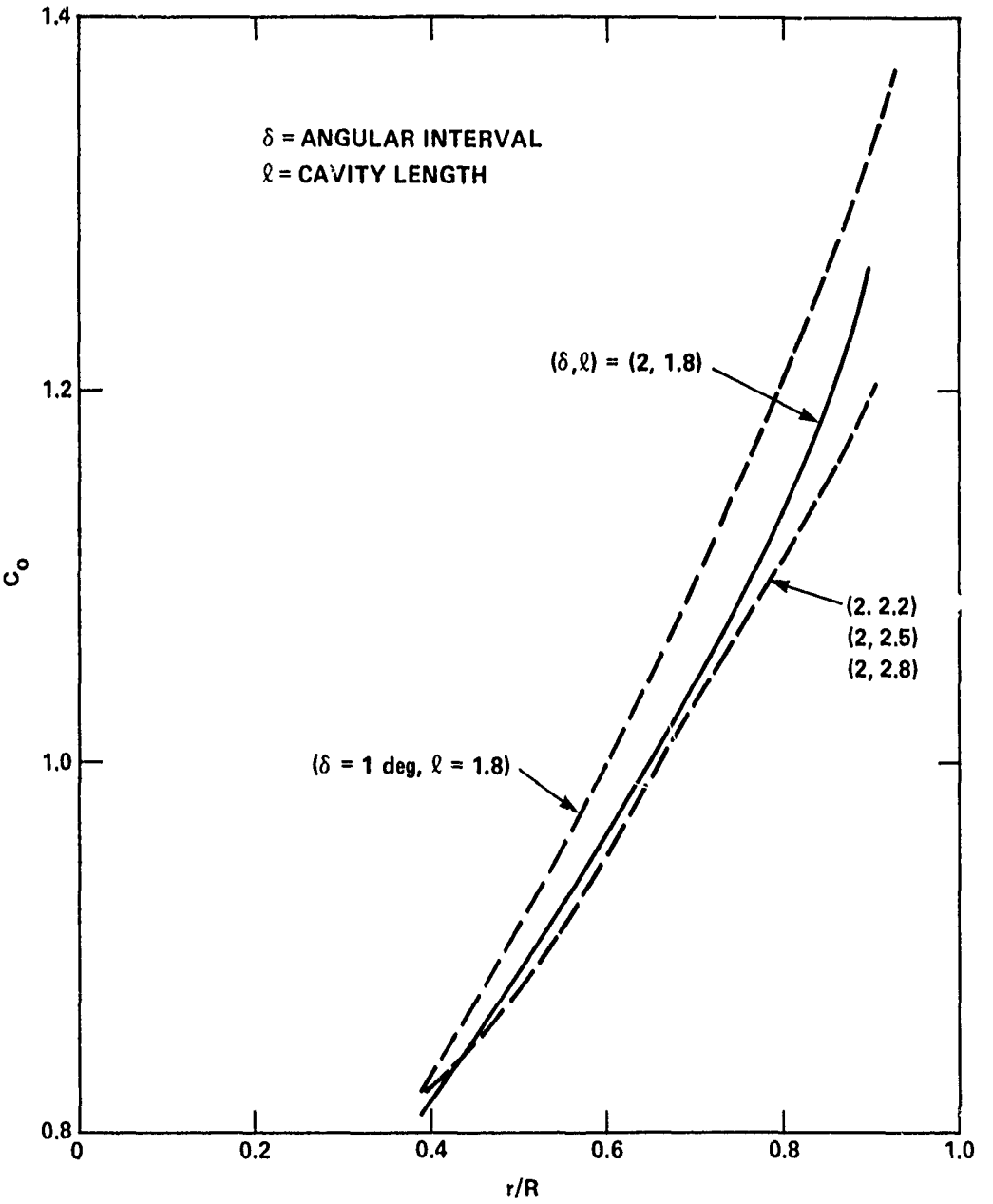

Figure 5 - Computed Camber Correction Factors c_o of Supercavitating Propeller Model 4717 for Different Angular Intervals δ and Cavity Truncation Points ℓ

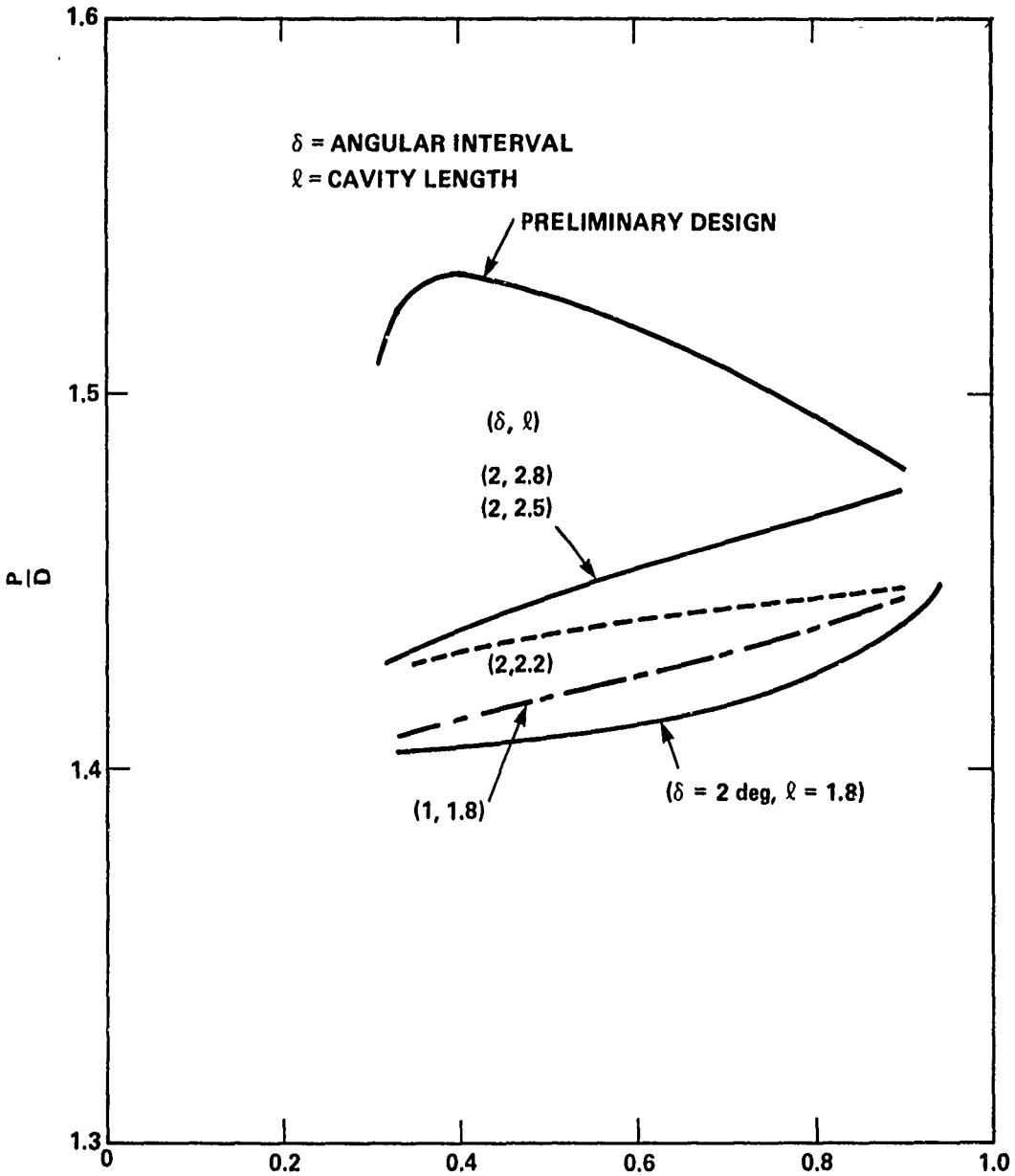

Figure 6 - Computed Pitch-Diameter Ratio of Supercavitating Propeller Model 4717 for Different Angular Intervals δ and Cavity Truncation Points ℓ

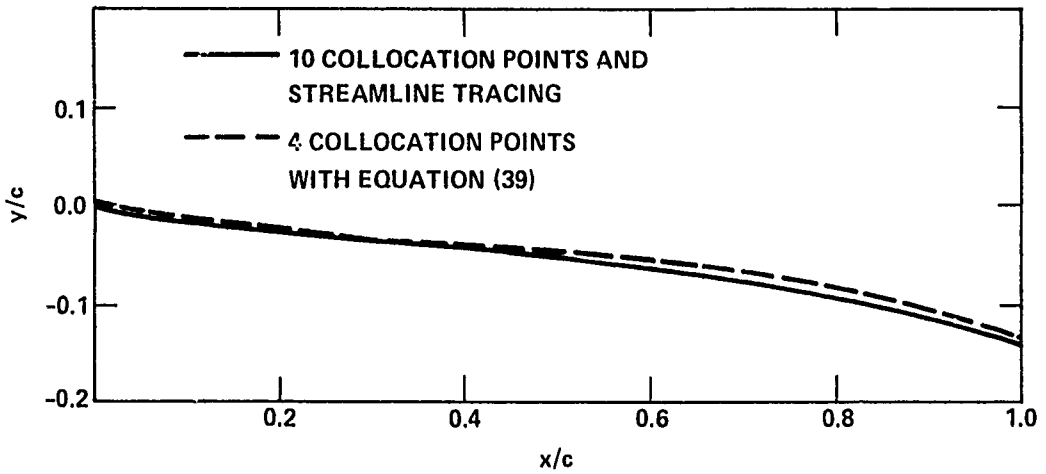

Figure 7 - Computed Shape of Blade Face of Model 4717 at r/R = 0.8 for Two Numbers of Collocation Points

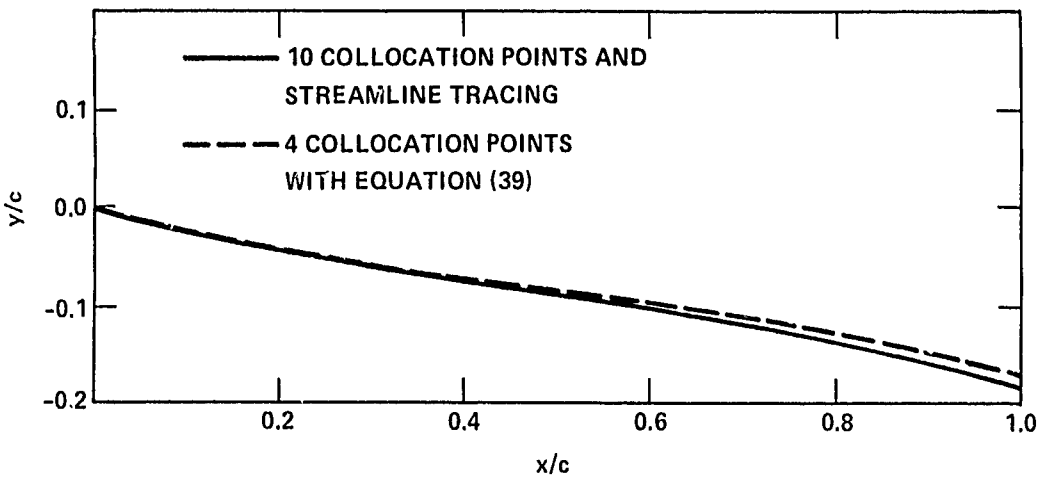

Figure 8 - Computed Shape of Blade Face of Model 4717 at r/R = 0.3978 for Two Numbers of Collocation Point

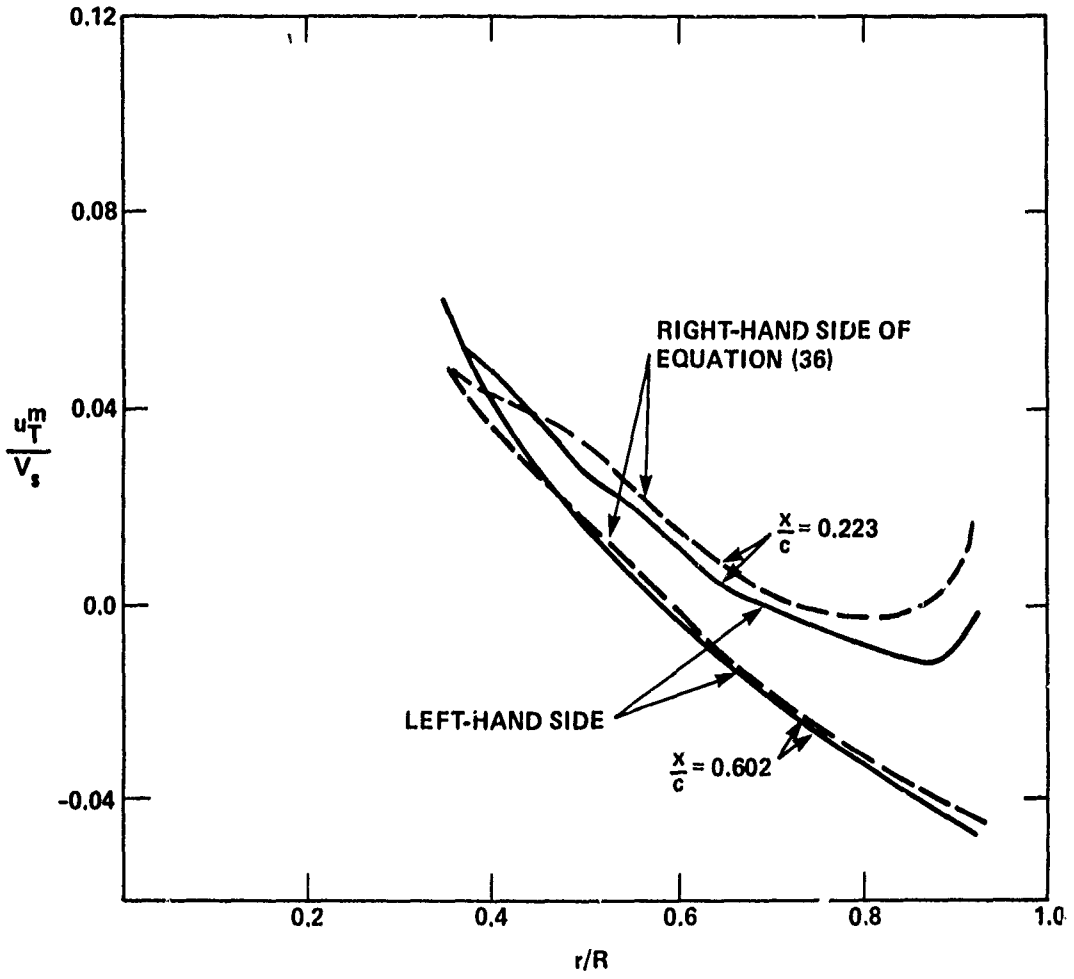

Figure 9 - Cavity Boundary Conditions without Hub Image and with Cubic Polynomial Source of Model 4717

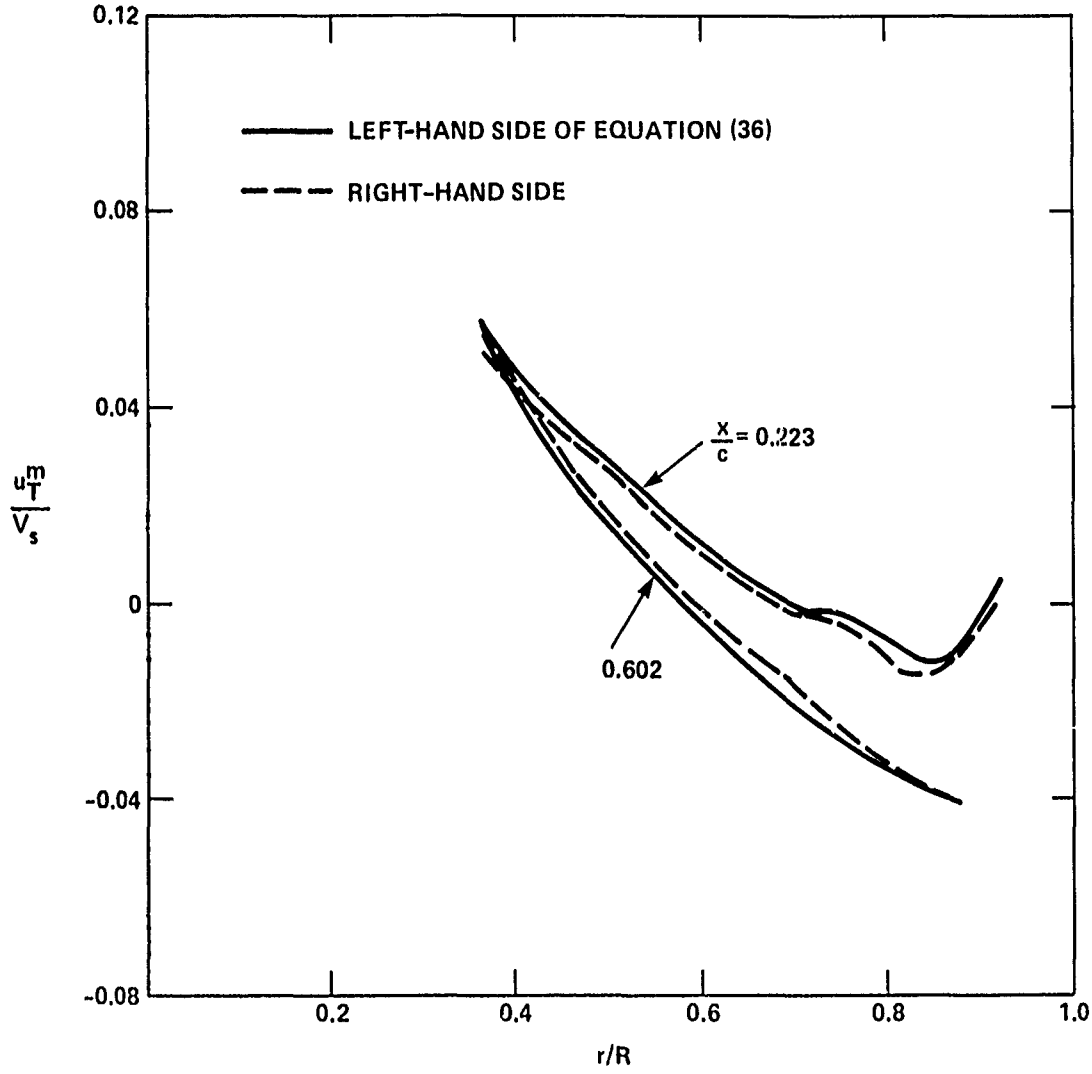

Figure 10 - Cavity Boundary Condition with 5-Degree Polynomial and without Hub Image of Model 4717

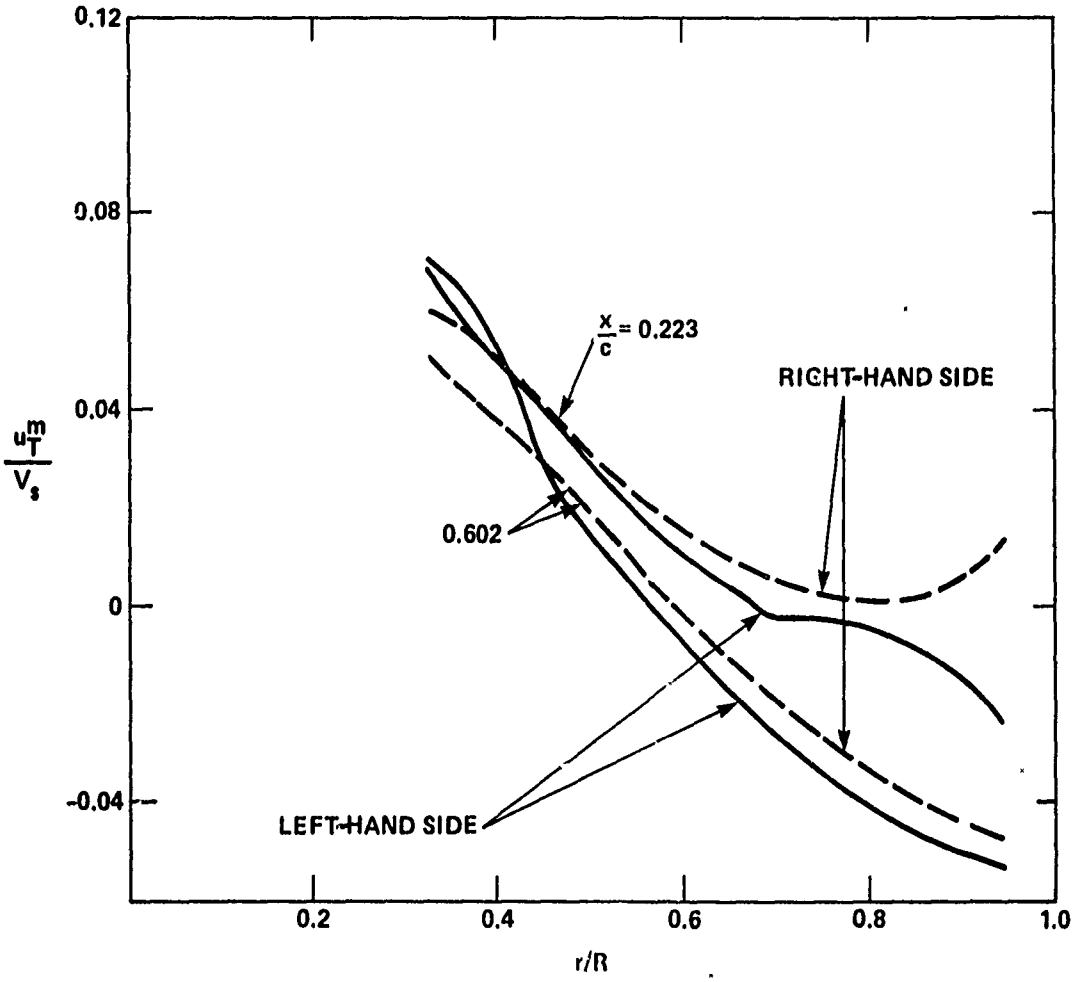

Figure 11 - Cavity Boundary Condition with Hub Images and Cubic Polynomial Source of Model 4717

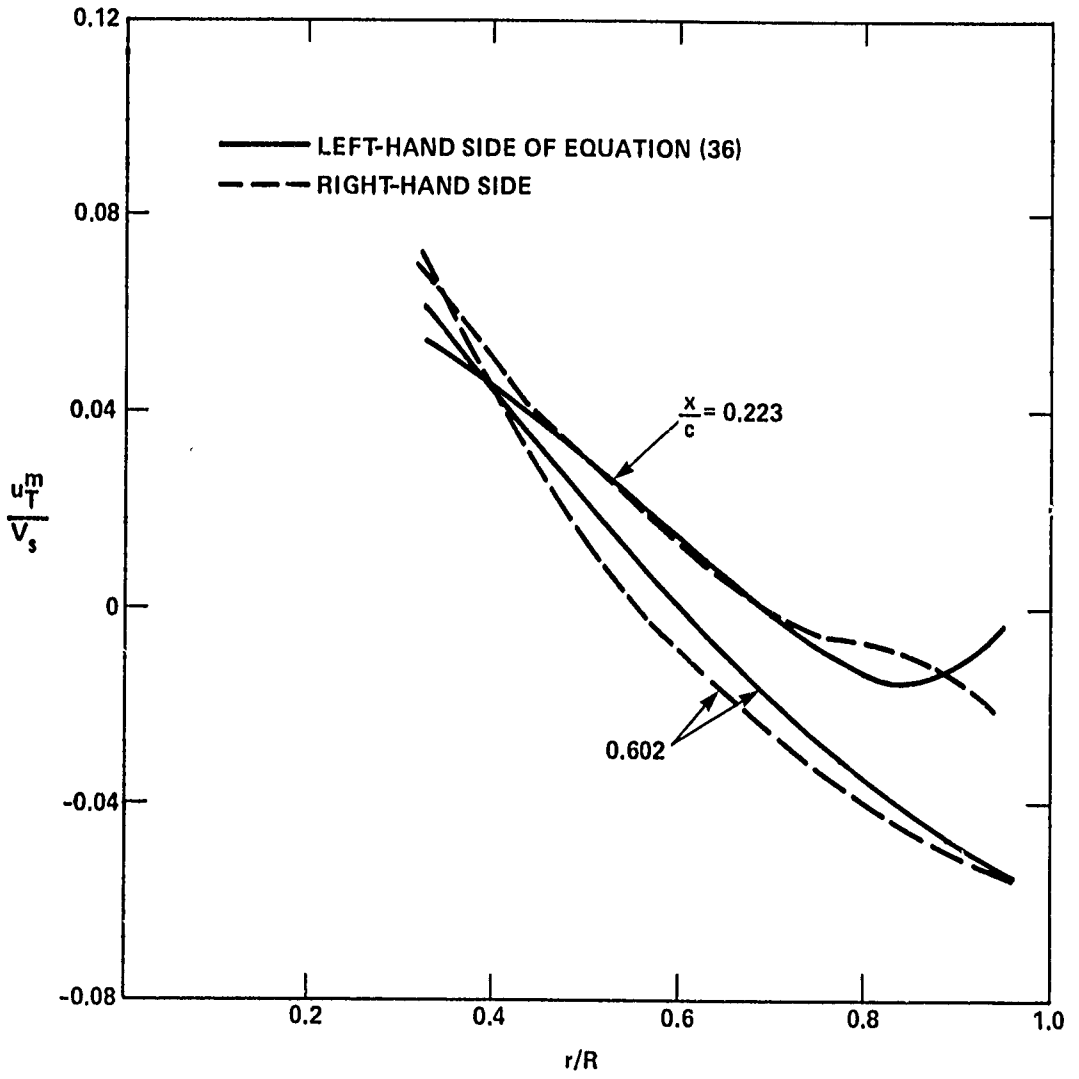

Figure 12 - Boundary Condition on Cavity with 5-Degree Polynomial and Hub Images of Model 4717

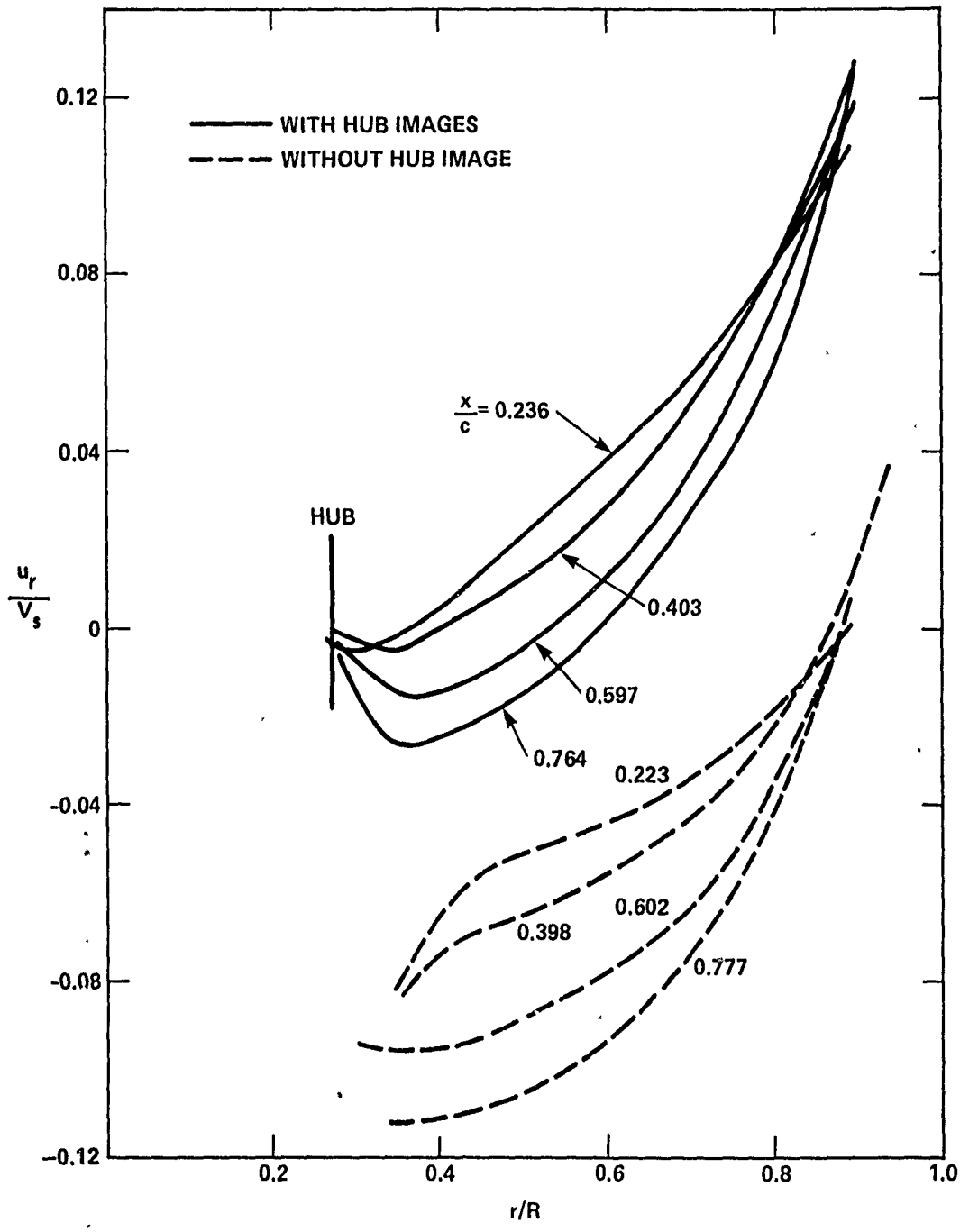

Figure 13 - Radial Component of Velocity with Cubic Polynomial Source of Model 4717

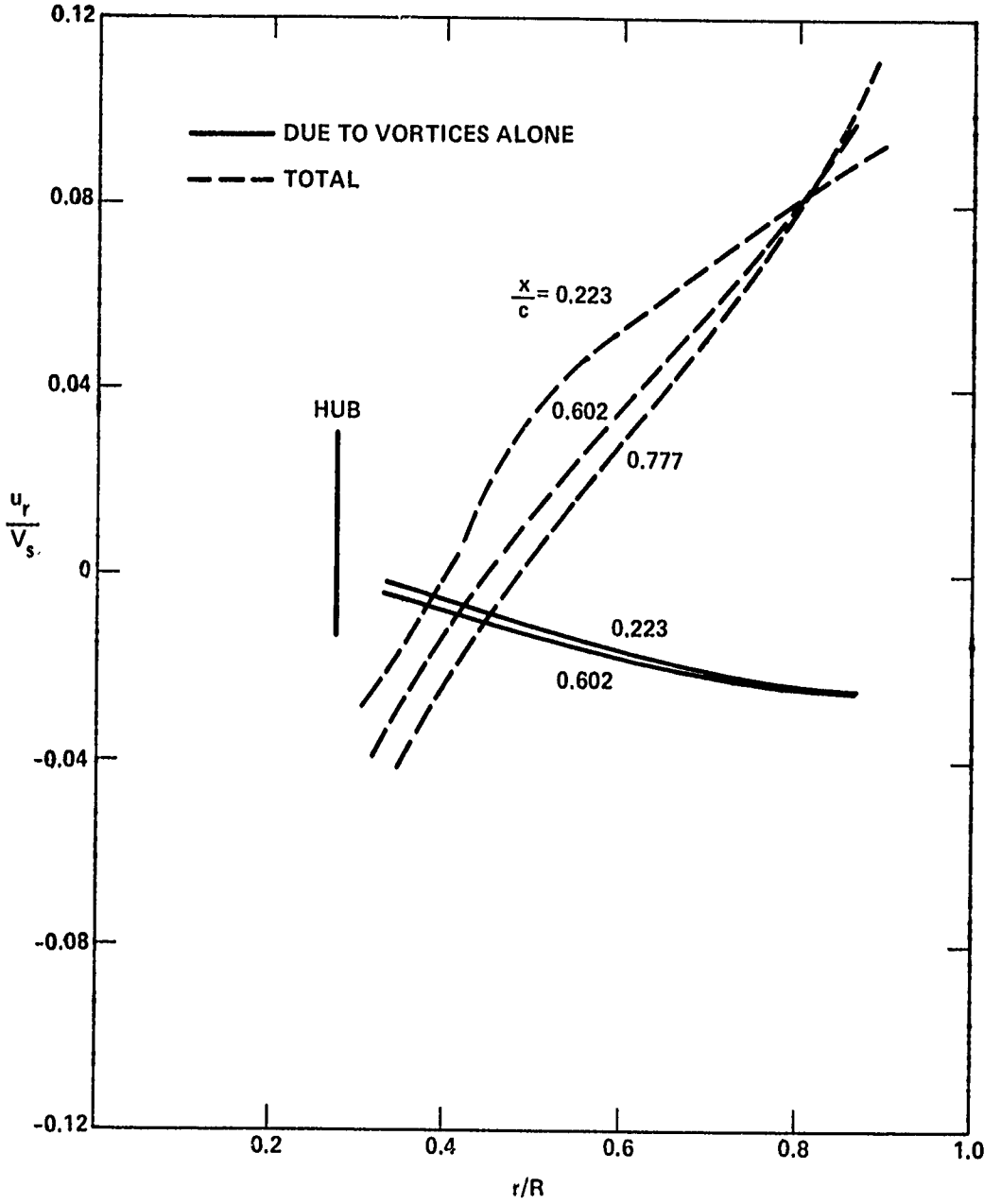

Figure 14 - Radial Component of Velocity with 5-Degree Polynomial Source without Hub Image of Model 4717

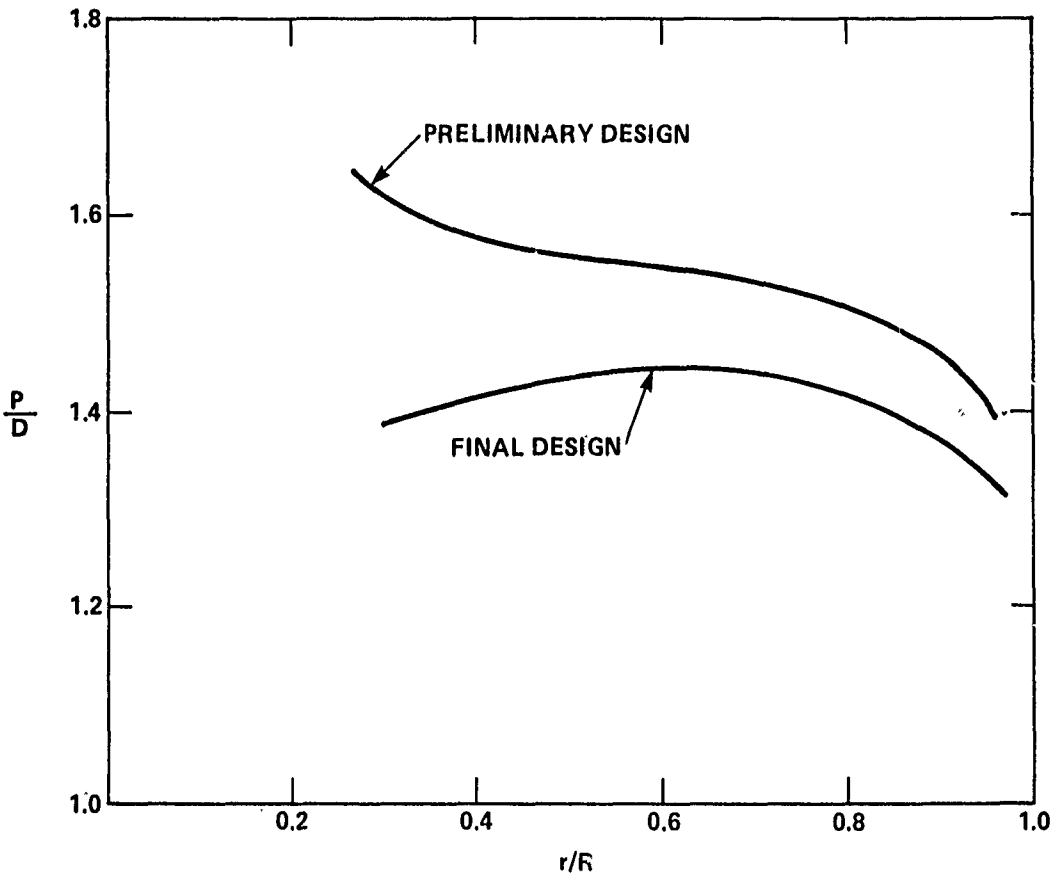

Figure 15 - Computed Pitch-Diameter Ratio of Model 4717 with Hub Image

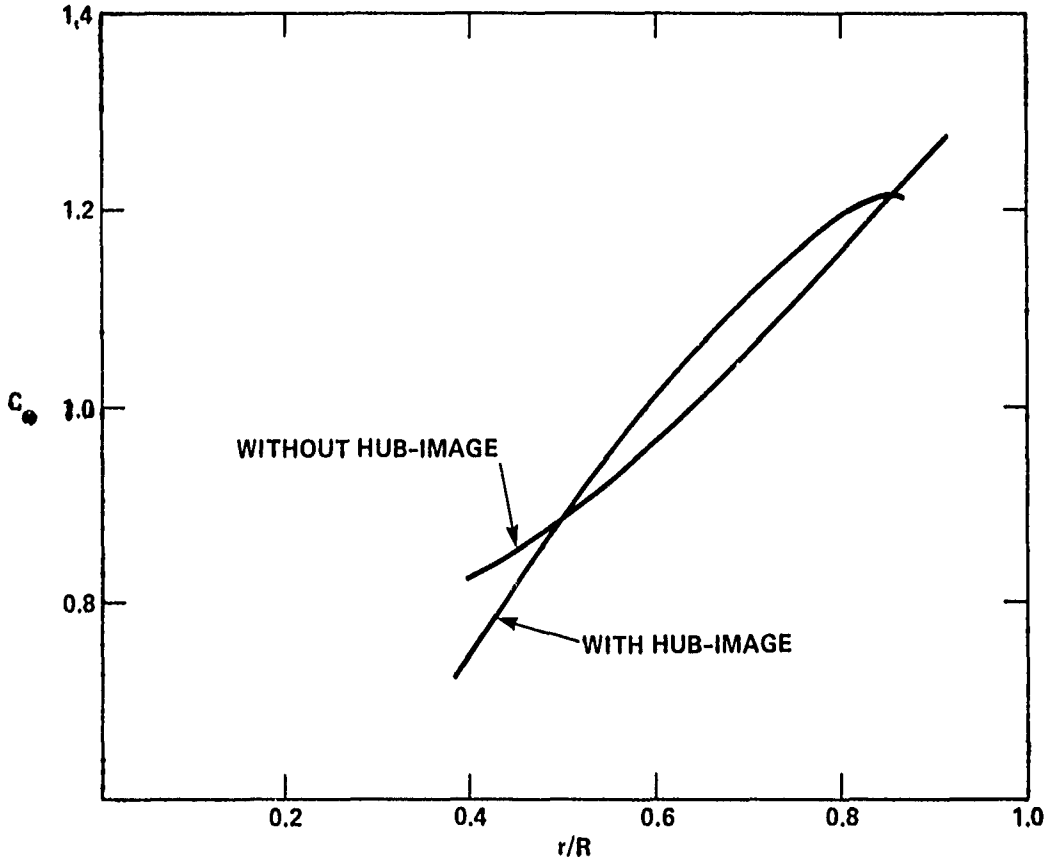

Figure 16 - Camber Correction Factor c_o of Model 4717 with Hub Image, δ = 2 Degrees and ℓ = 2.5

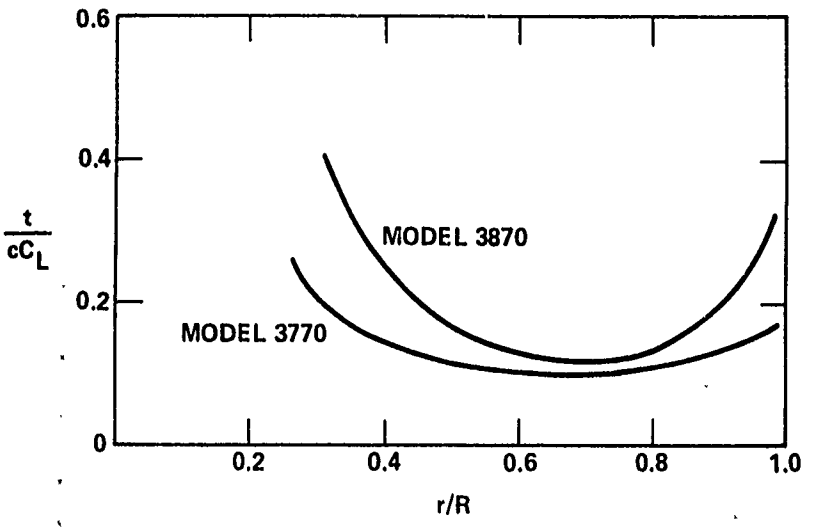

Figure 17 - Design Cavity Thickness $t/(cC_L)$ at Leading Edge x/c = 0.1

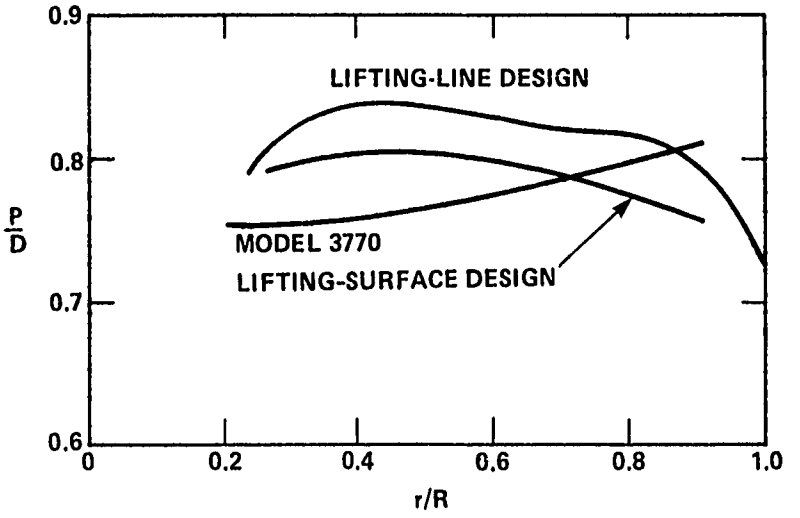

Figure 18 - Pitch-Diameter Ratio of Model 3770 with Leading-Edge Point Drag (Case 1)

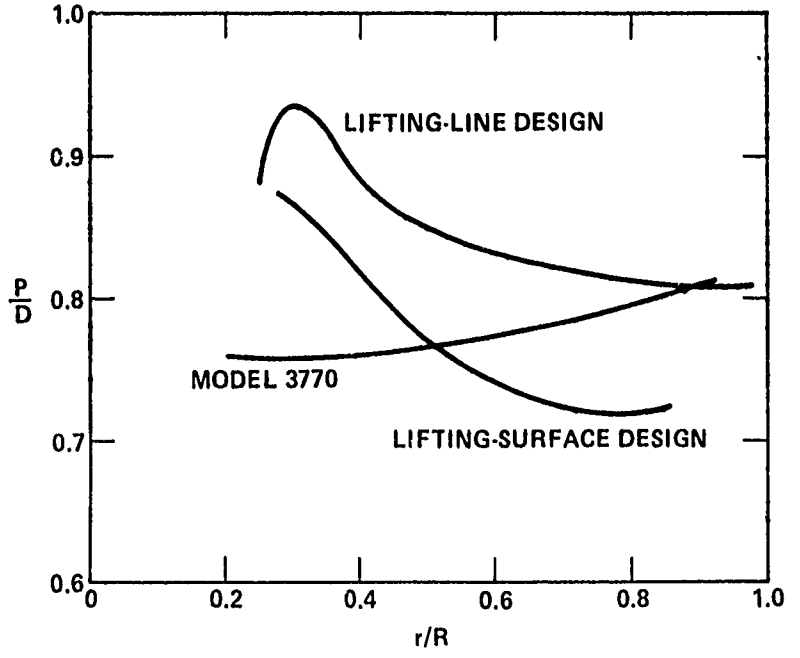

Figure 19 - Pitch-Diameter Ratio of Model 3770 without Leading-Edge Point Drag (Case 2)

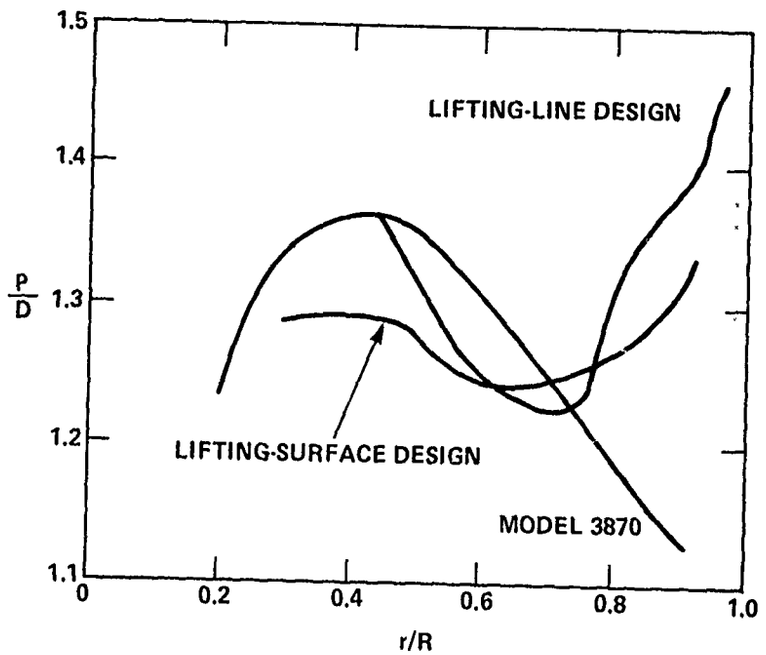

Figure 20 - Pitch-Diameter Ratio of Model 3870 (Case 1)

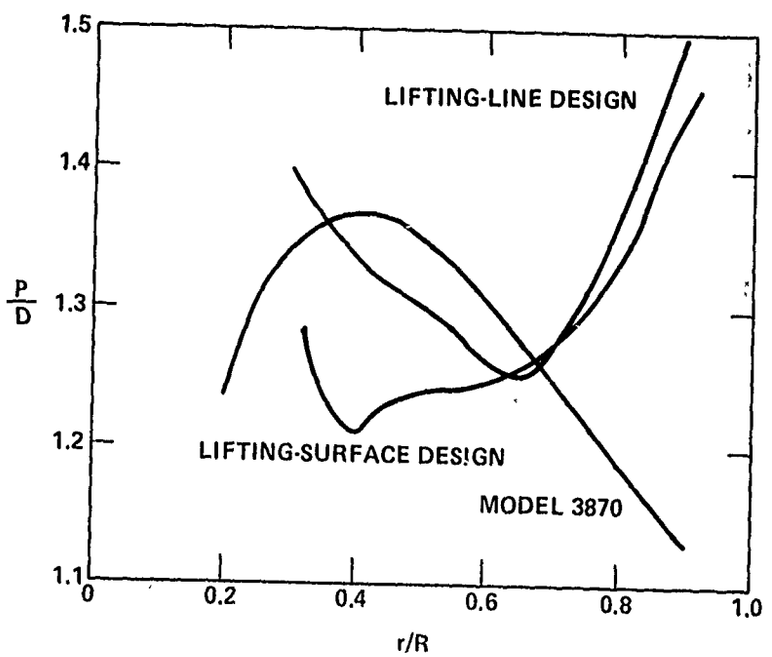

Figure 21 - Pitch-Diameter Ratio of Model 3870 (Case 2)

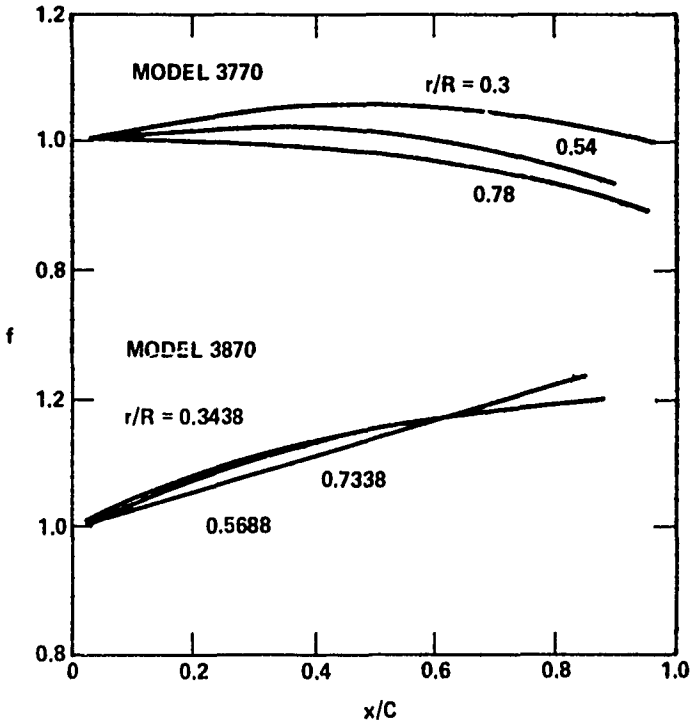

Figure 22 - Lifting-Surface Source Correction Factors (Case 2)

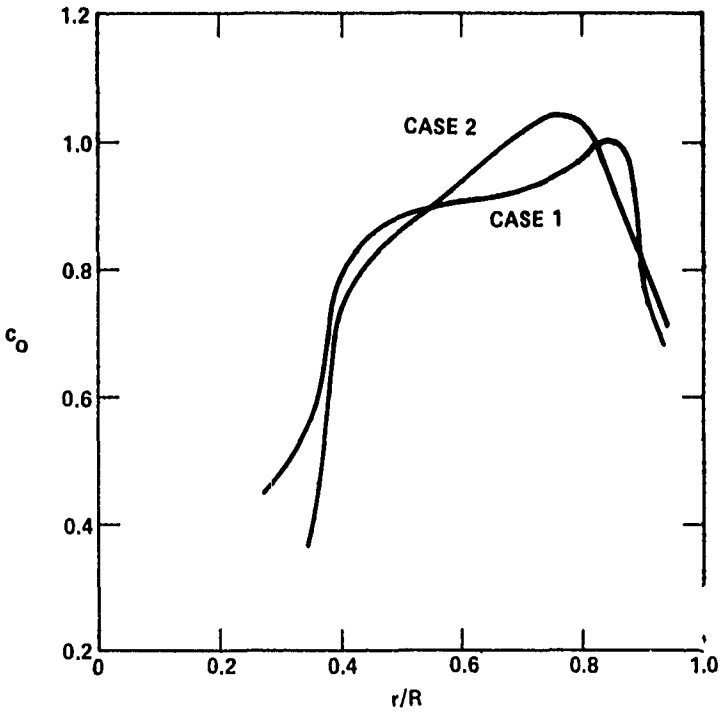

Figure 23 - Camber Correction Factor c_o of Model 3770

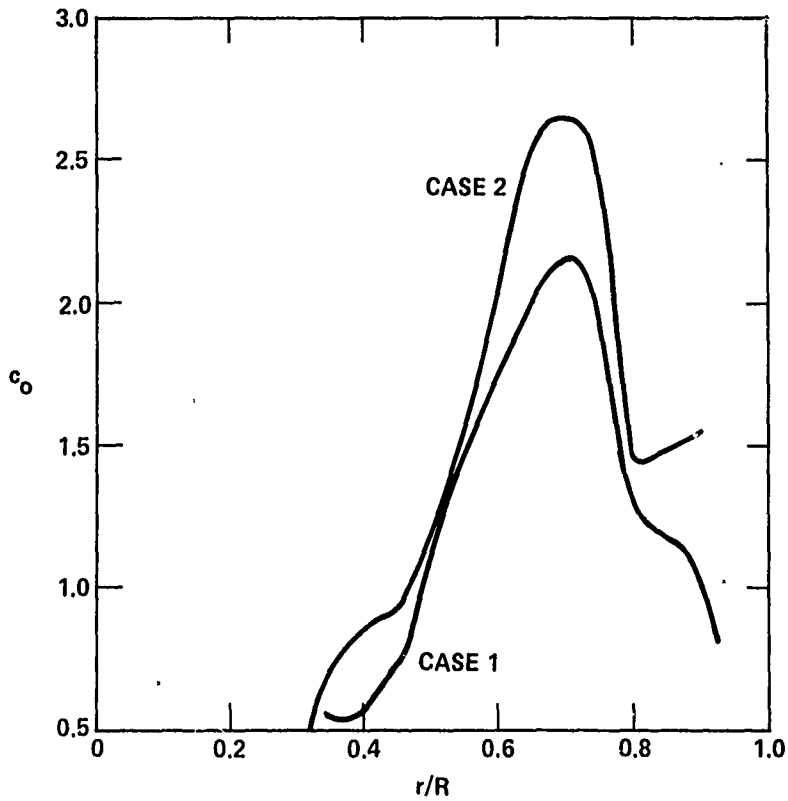

Figure 24 - Camber Correction Factor c_o of Model 3870

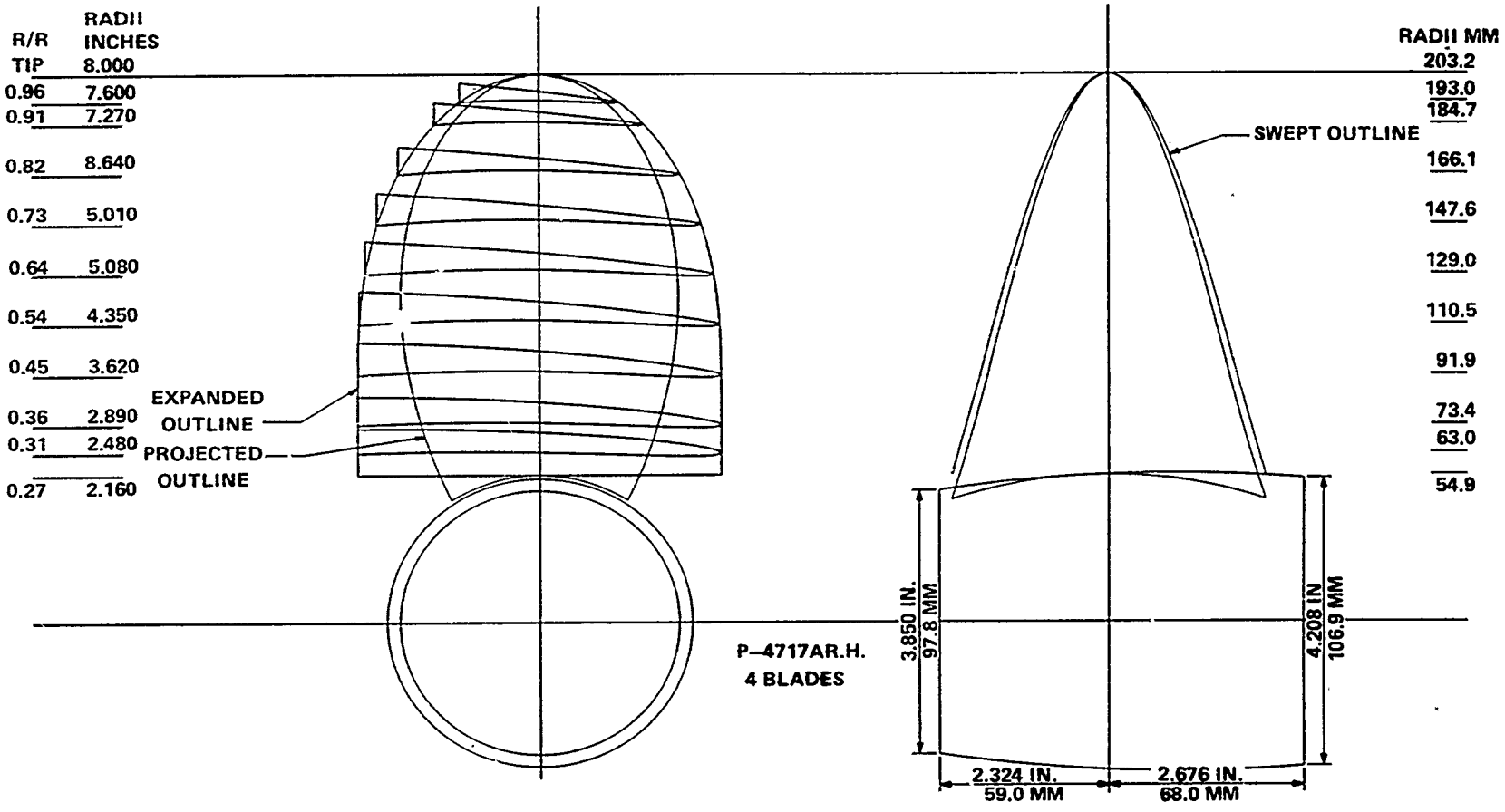

Figure 25 - Drawing of Propeller 4717C

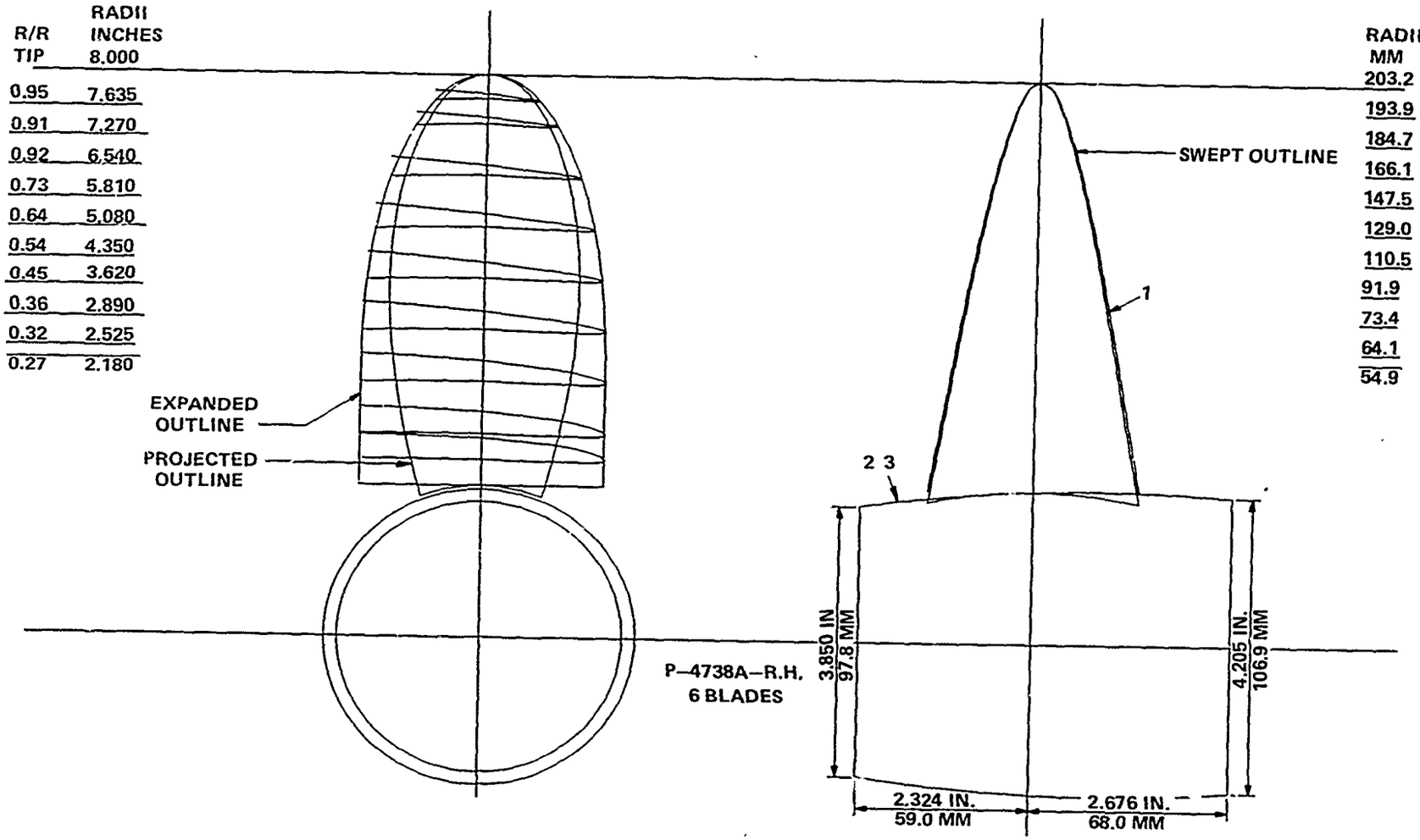

Figure 26 - Drawing of Propeller 4738A

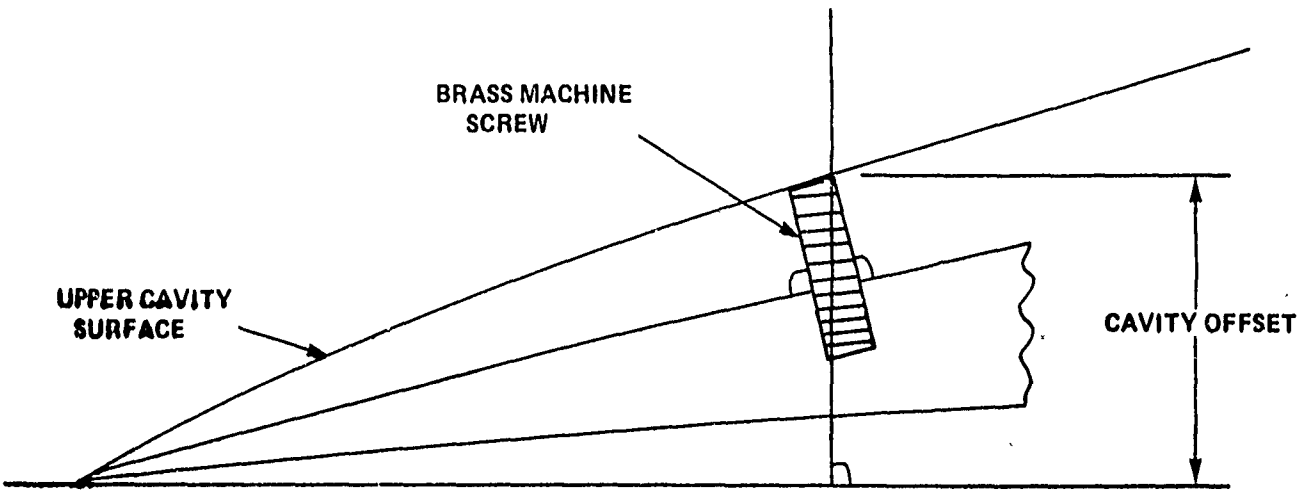

Figure 27 - Placement of Brass Pin Perpendicular to Back of Blade

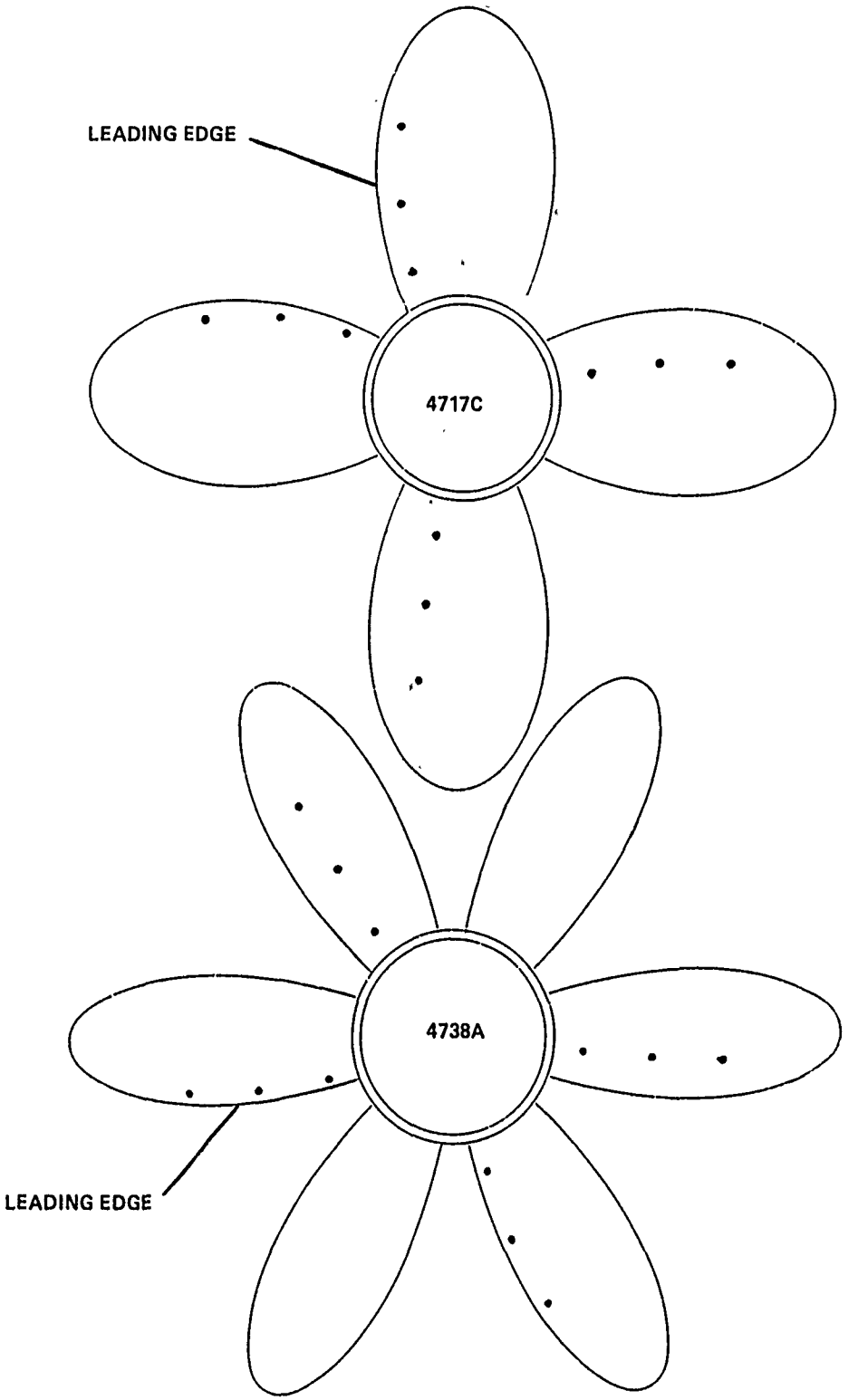

Figure 28 - Pin Locations at 10, 30, 60 and 90 Percent of Chord at Non-Dimensional Radii (r/R) Values of 0.361, 0.544, and 0.726 for Propellers 4717C and 4738A

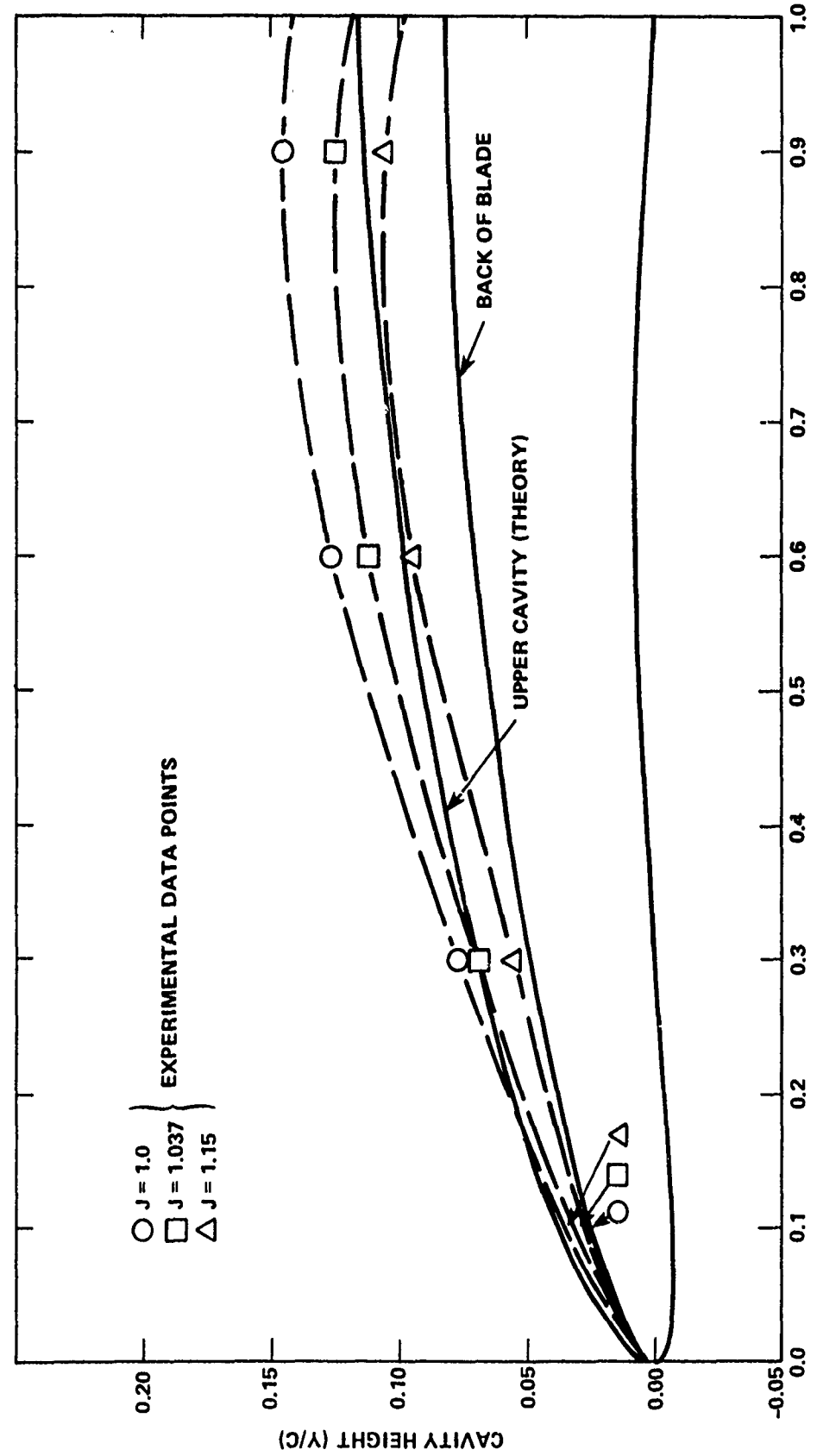

Figure 29 - Comparison of Theoretical and Empirical Cavity Shapes at r/R = 0.361 for Propeller 4717C

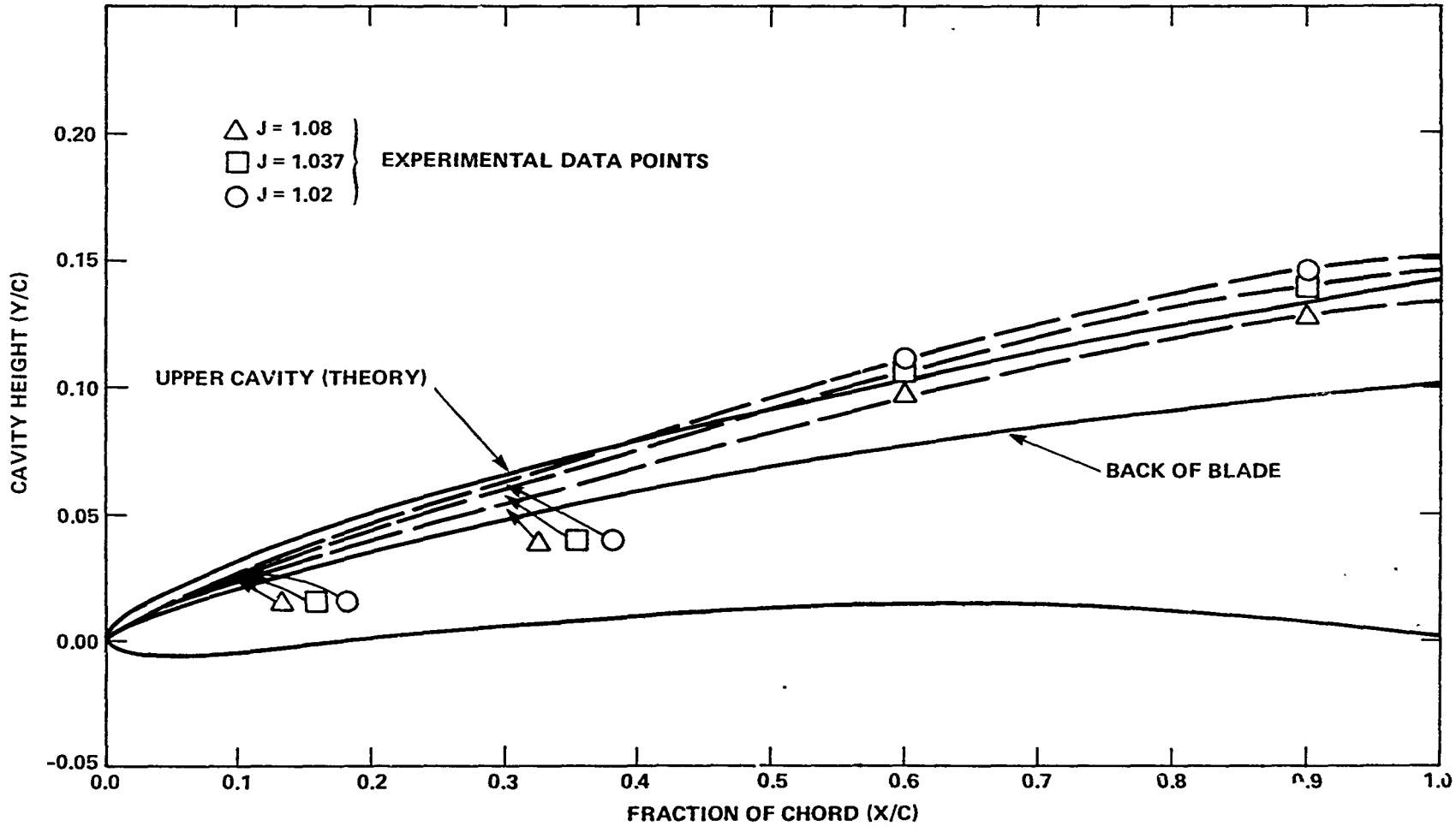

Figure 30 - Comparison of Theoretical and Empirical Cavity Shapes at r/R = 0.544 for Propeller 4717C

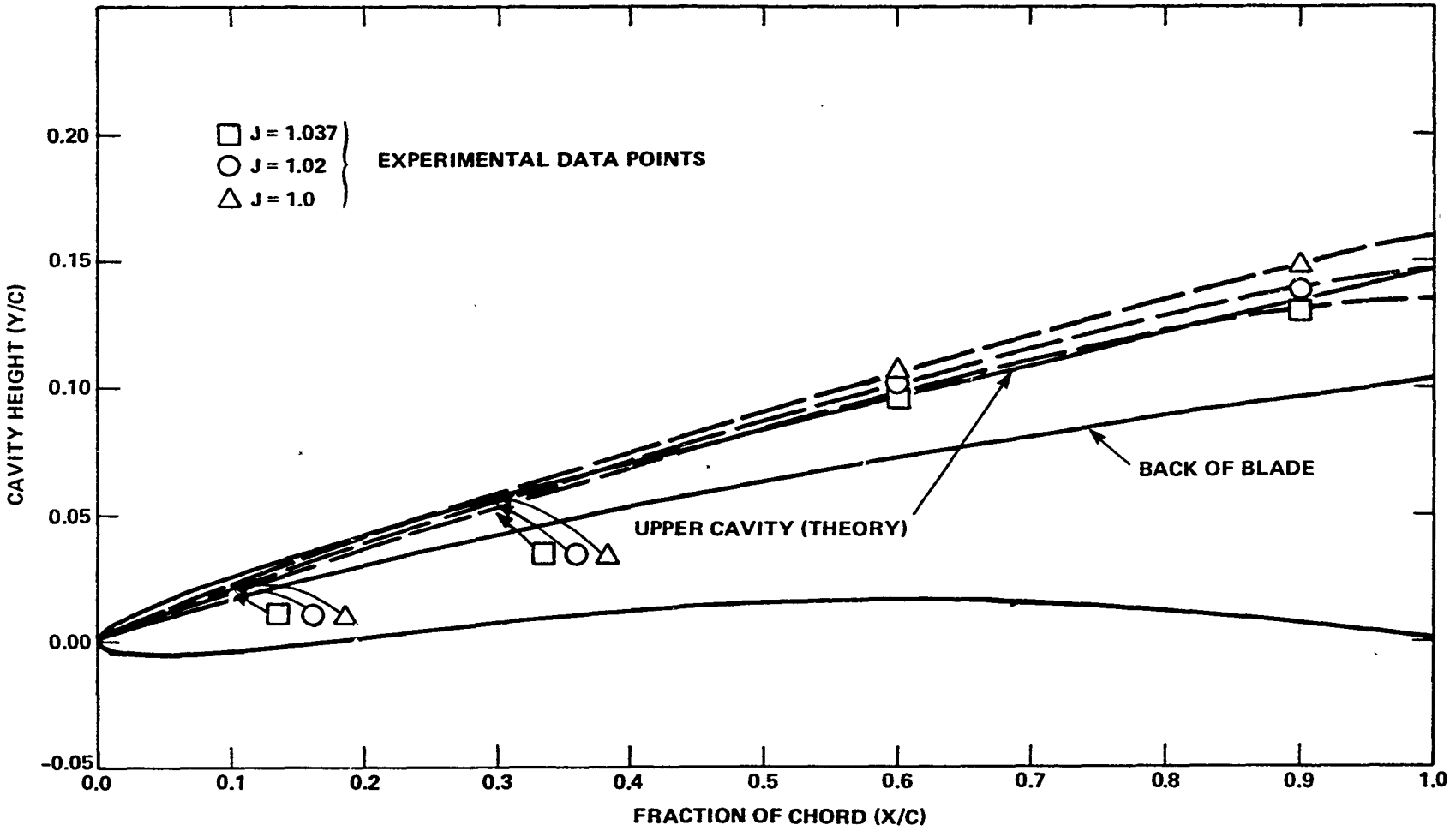

Figure 31 – Comparison of Theoretical and Empirical Cavity Shapes at r/R = 0.726 for Propeller 4717C

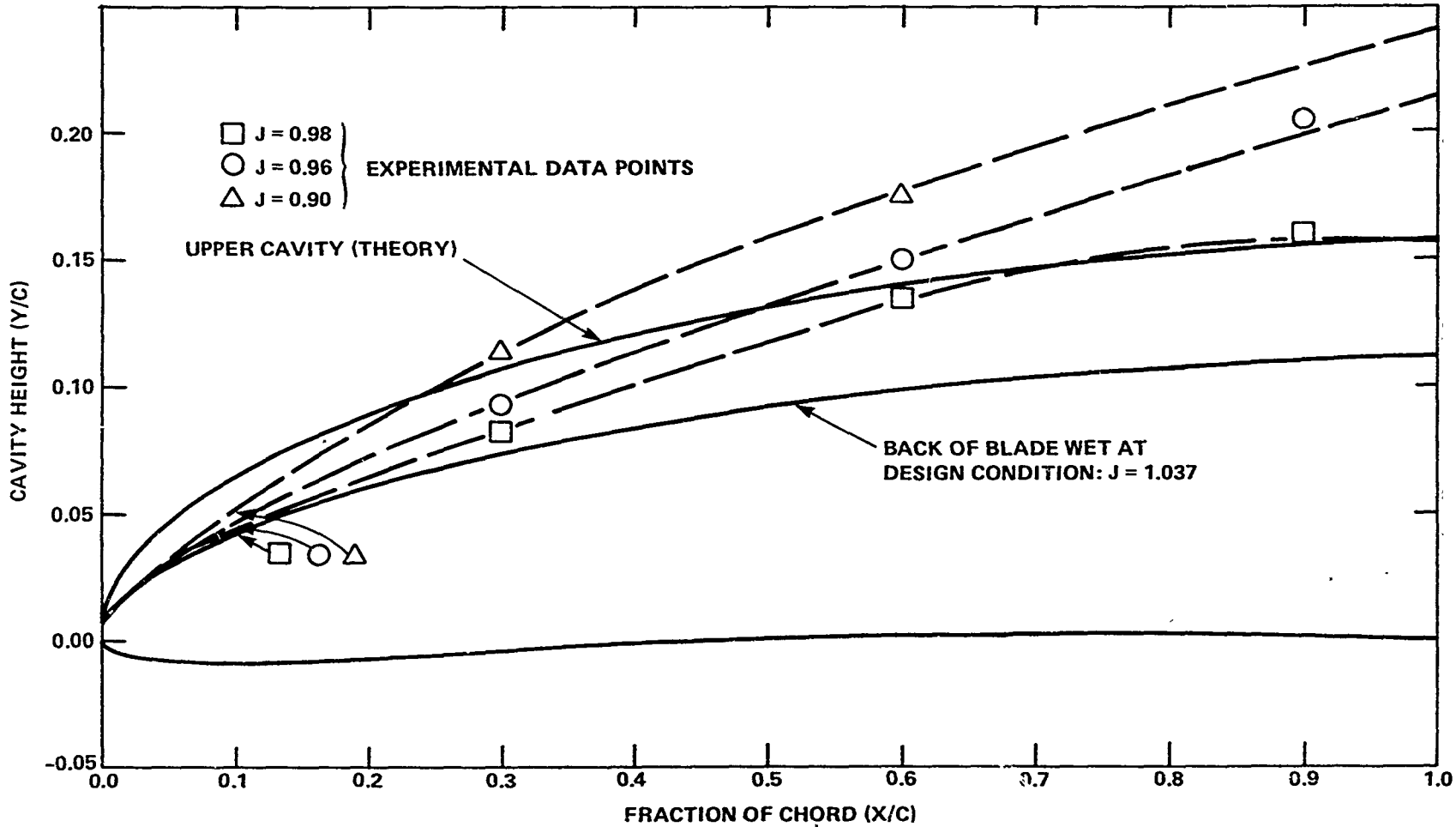

Figure 32 - Comparison of Theoretical and Empirical Cavity Shapes at r/R = 0.361 for Propeller 4738A

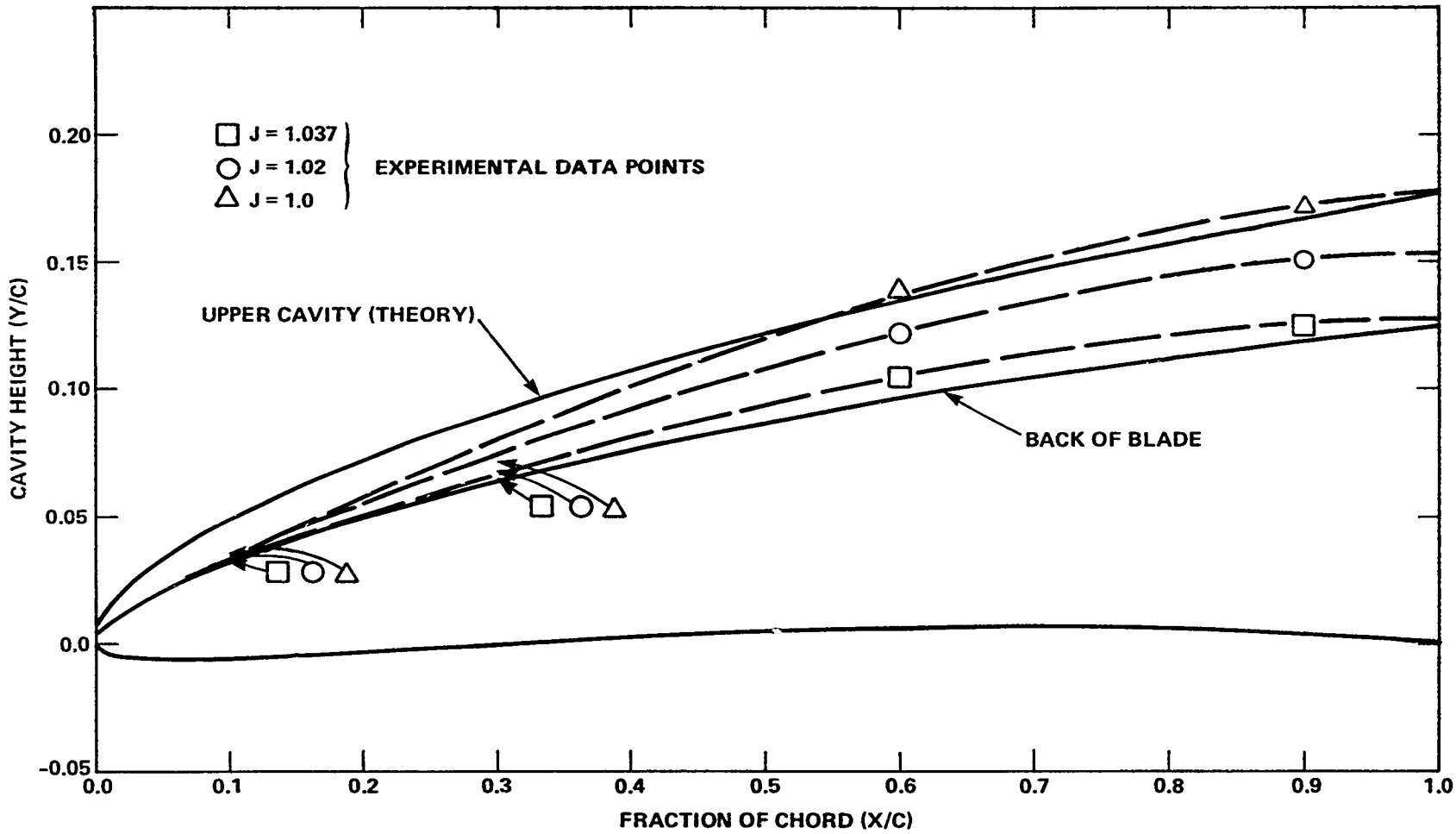

Figure 33 - Comparison of Theoretical and Empirical Cavity Shapes at r/R = 0.544 for Propeller 4738A

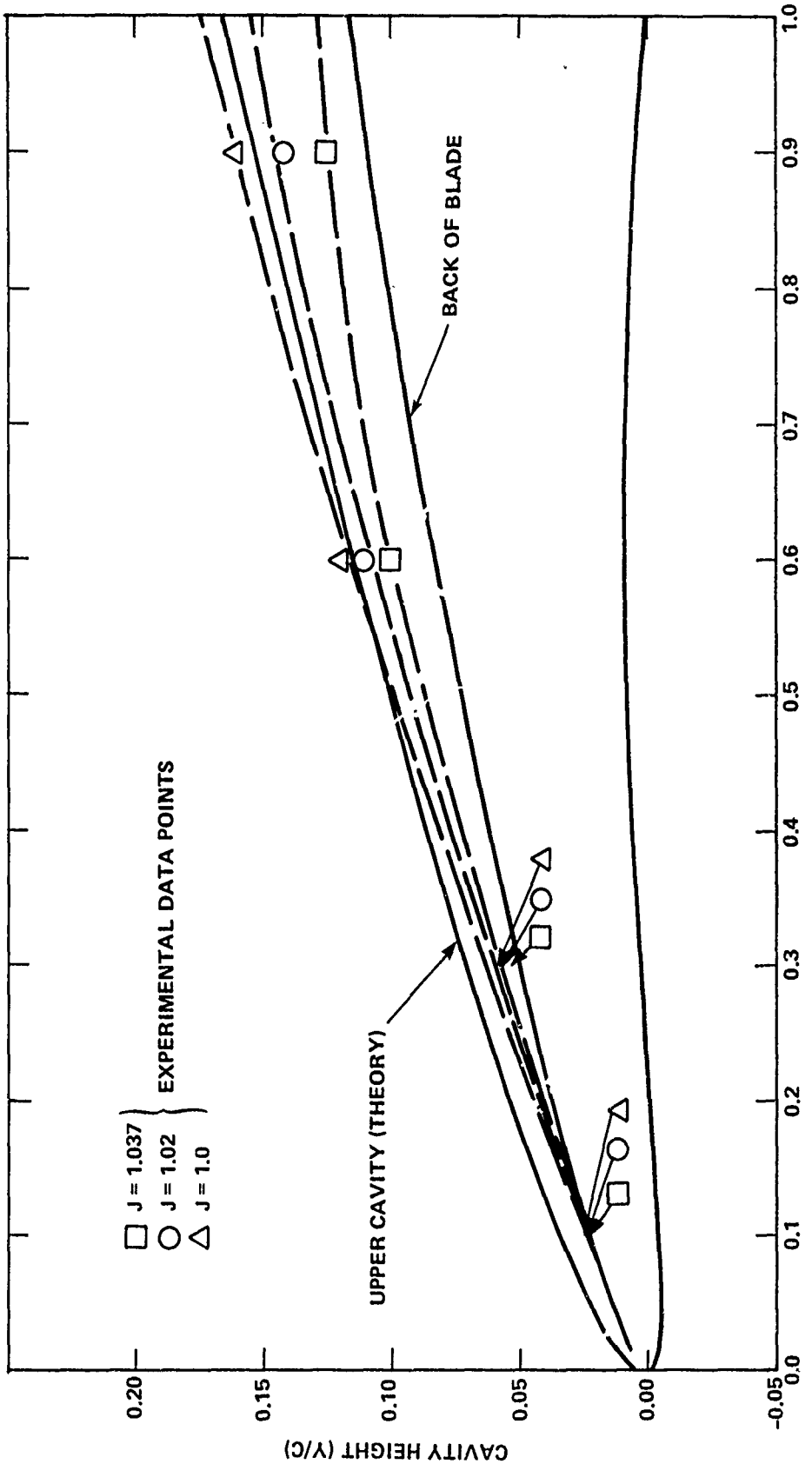

Figure 34 - Comparison of Theoretical and Empirical Cavity Shapes at r/R = 0.726 for Propeller 4738A

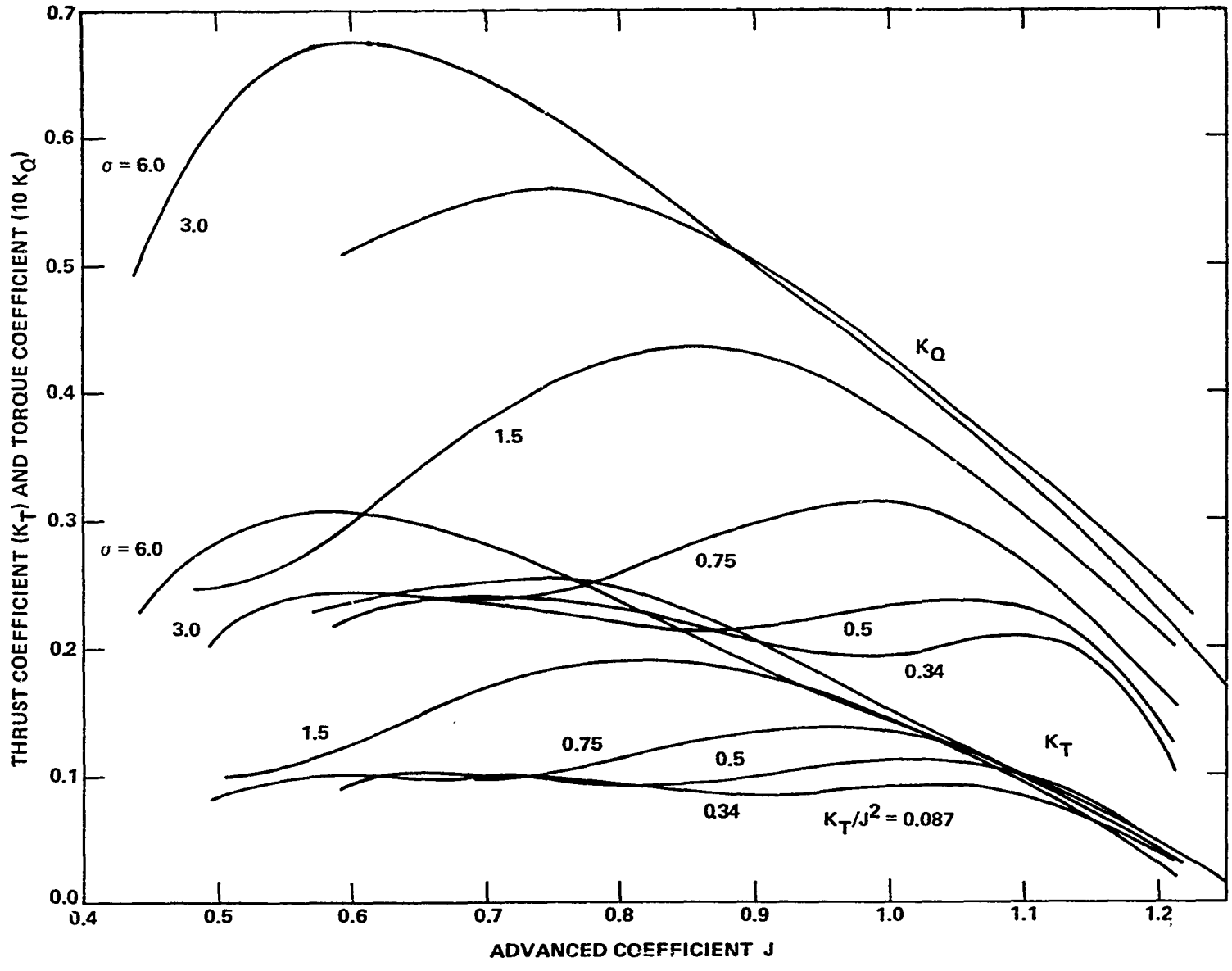

Figure 35 - Cavitation Performance of Propeller 4738A

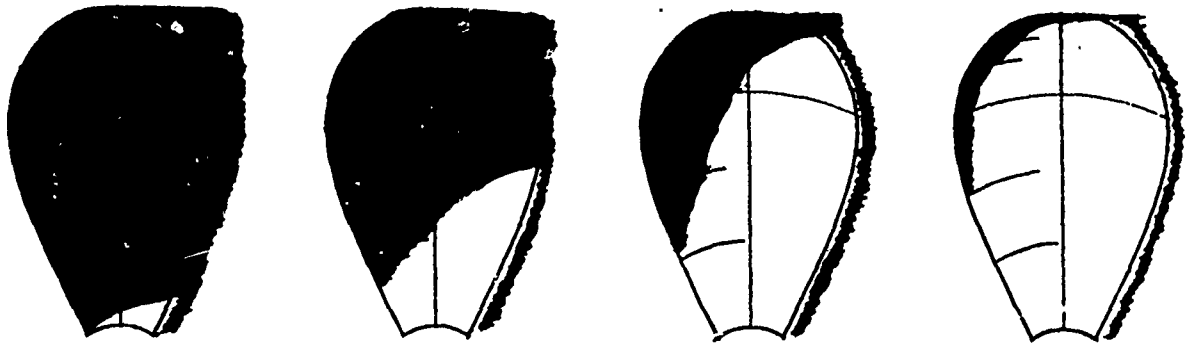

J = 0.5 0.6 0.7 0.8

σ = 3.0

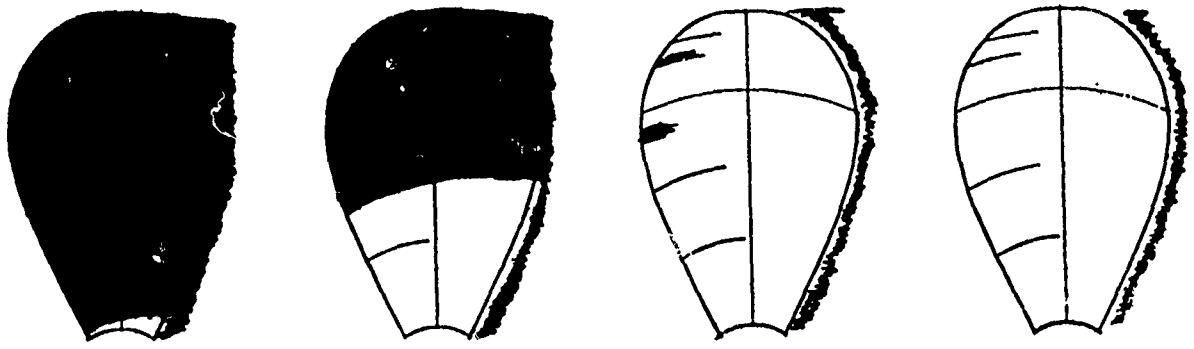

J = 0.9 1.0 1.04 1.1

σ = 0.34

Figure 36 - Sketches of Cavitation Present on the Back of Propeller 4717B at Two Cavitation Numbers

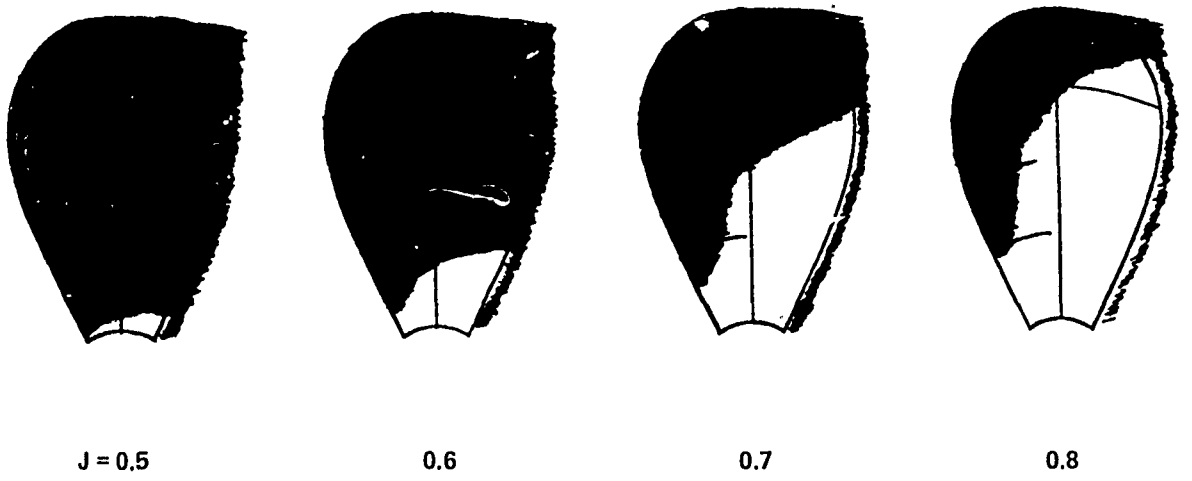

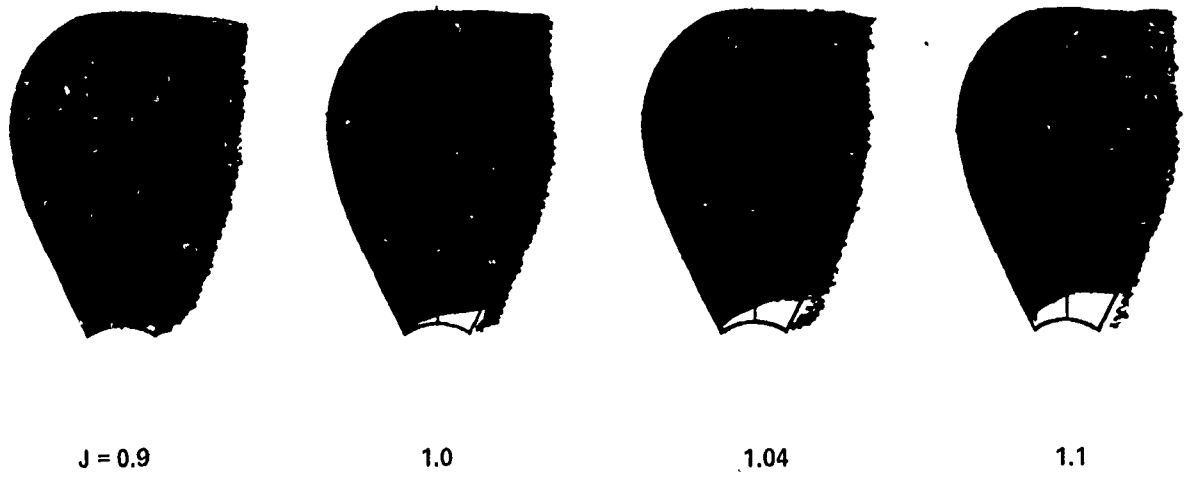

Figure 37 - Sketches of Cavitation Present on the Back of Propeller 4717C at Two Cavitation Numbers

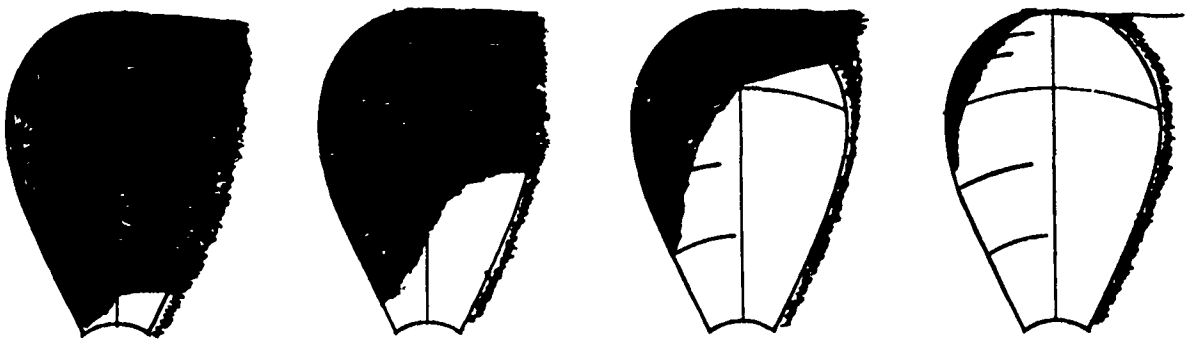

J = 0.6 0.7 0.8 0.9

σ = 3.0

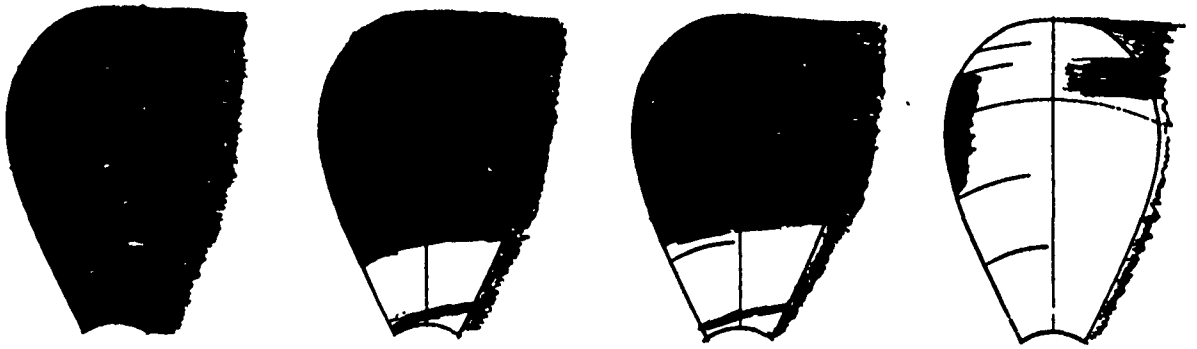

J = 0.9 1.0 1.04 1.1

σ = 0.34

Figure 38 - Sketches of Cavitation Present on the Back of Propeller 4738A at Two Cavitation Numbers

TABLE 1 - PROPELLER DESIGN PREDICTIONS

Propeller Number	4717C	4738A
V_s	58.84	58.84 knots (30.35 m/sec)
n	1000	1000
K_T	0.092	0.092
J	1.037	1.037
Z	4	6
$P/D_{0.7}$	1.416	1.410
σ	0.34	0.34
η	0.67	0.67

TABLE 2 - DESIGN AND PERFORMANCE CHARACTERISTICS OF SUPERCAVITATING PROPELLERS

Propeller	Model 3770[2]	Model 3870[2]
Z	3	4
P/D (0.7)	0.786	1.243
EAR	0.508	0.727
c/2 (0.7)	0.351	0.344
Experiment J	0.44	0.834
Experiment σ	0.617	0.45
Experiment K_T	0.075*	0.115
Experiment η	52.0	59.4
by Venning and Haberman[2] Preliminary Design[2] (Lifting-Line Theory)	0.1004	0.1402
Lifting-Surface Design	0.075	0.115
Case 1**	0.073	0.114
Case 2**	0.073	0.114
by Venning and Haberman[2] Preliminary Design[2]	54.1	64.0
Case 1**	50.1	58.2
Case 2**	50.5	56.7
Lifting-Surface Design		
Case 1	47.8	58.7
Case 2	50.4	58.9

[2]Venning and Haberman.

*A corrected value of K_T as given in Reference 2.

**Case 1 - without angle of attack; Case 2 - preset angle of attack.

TABLE 3 - PROPELLER DESIGN CRITERIA

Power, maximum continuous	16,000 hp (11,931 kW) for two propellers
$1 - t$	0.925
$1 - w_t$	0.870
Shaft Centerline at Design Speed	6.82 ft (2.079 m)
Maximum D	5 ft (1.524 m)
No. of Blades	4, 6
Design Objective	maximum speed
Minimum Rotative Speed	750 rpm
Hump Thrust Margin	20 percent

TABLE 4 - MODEL PROPELLER GEOMETRY*

Design Parameters	Propeller Number	
	4717C	4738A
Z	4	6
Diameter, in. (cm)	16.000 (40.64)	16.000 (40.64)
Pitch,** in. (cm)	22.656 (57.546)	22.560 (57.302)
P/D**	1.416	1.410
EAR	0.495	0.492
Chord length,** in. (cm)	4.560 (11.582)	3.017 (7.663)

*Interpreted from drafting room offsets.

**At 0.7R.

TABLE 5 - SCOPE OF EXPERIMENTS

Propeller Number								
4717B			4717C			4738A		
σ	V*	J	σ	V*	J	σ	V*	J
			6.0	15.0	0.45-1.3	6.0	15.0	0.45-1.3
3.0	30.0	0.5-1.2	3.0	30.0	0.5-1.2	3.0	30.0	0.5-1.2
1.5	30.0	0.5-1.2	1.5	30.0	0.5-1.2	1.5	30.0	0.5-1.2
0.75	30.0	0.5-1.2	0.75	30.0	0.5-1.2	0.75	30.0	0.5-1.2
						0.5	30.0	0.6-1.2
0.3	35.0	0.7-1.2	0.34	35.0	0.7-1.2	0.34	35.0	0.7-1.2

*In feet per second.

TABLE 6 - CAVITATION PERFORMANCE OF PROPELLER 4717B

SIGMA (σ)* = 3.000				SIGMA* = 1.500			
J	K_T	10KQ	η	J	K_T	10KQ	η
.5000	.2014	.4583	.3497	.5000	.1134	.2808	.3213
.5500	.2218	.5186	.3744	.5500	.1224	.2997	.3576
.6000	.2329	.5450	.4080	.6000	.1421	.3388	.4003
.6500	.2334	.5491	.4398	.6500	.1623	.3802	.4417
.7000	.2238	.5395	.4622	.7000	.1770	.4126	.4778
.7500	.2055	.5219	.4701	.7500	.1826	.4302	.5068
.8000	.1807	.5000	.4602	.8000	.1783	.4312	.5264
.8500	.1520	.4755	.4324	.8500	.1648	.4174	.5339
.9000	.1220	.4491	.3893	.9000	.1440	.3925	.5256
.9500	.0931	.4203	.3350	.9500	.1196	.3608	.4969
1.0000	.0670	.3865	2743	1.0000	.0910	.3267	.4434
1.0500	.0442	.3533	.2090	1.0500	.0633	.2931	.3608
1.1000	.0241	.3146	.1341	1.1000	.0360	.2602	.2424
1.1500	.0042	.2736	.0283	1.1500	.0082	.2249	.0671
1.2000	-.0199	.2329	-.1632	1.2000	-.0236	.1789	-.2515
SIGMA* = 0.750				SIGMA* = 0.340			
.5000	.0920	.2333	.3138	.7000	.0967	.2516	.4281
.5500	.0968	.2525	.3357	.7500	.1024	.2663	.4592
.6000	.0987	.2600	.3623	.8000	.0941	.2504	.4786
.6500	.1020	.2668	.3955	.8500	.0854	.2337	.4943
.7000	.1083	.2778	.4344	.9000	.0802	.2261	.5081
.7500	.1168	.2932	.4753	.9500	.0761	.2241	.5134
.8000	.1251	.3102	.5133	1.0000	.0677	.2173	.4957
.8500	.1302	.3241	.5433	1.0500	.0499	.1950	.4273
.9000	.1289	.3296	.5603	1.1000	.0214	.1528	.2451
.9500	.1188	.3220	.5579	1.1500	-.0119	.0992	-.2194
1.0000	.0987	.2988	.5259	1.2000	-.0337	.0617	******
1.0500	.0698	.2610	.4466				
1.1000	.0357	.2142	.2920				
1.1500	.0041	.1699	.0439				
1.2000	-.0134	.1473	-.1742				

*Cavitation number.

TABLE 7 - CAVITATION PERFORMANCE OF PROPELLER 4717C

SIGMA* = 3.000				SIGMA* = 1.500			
J	K_T	10KQ	η	J	K_T	10KQ	η
.5000	.2038	.4625	.3507	.5000	.1160	.2813	.3283
.5500	.2201	.5000	.3853	.5500	.1297	.3078	.3688
.6000	.2379	.5386	.4218	.6000	.1474	.3455	.4073
.6500	.2498	.5666	.4562	.6500	.1654	.3843	.4453
.7000	.2522	.5780	.4861	.7000	.1808	.4171	.4830
.7500	.2443	.5718	.5099	.7500	.1915	.4397	.5199
.8000	.2274	.5504	5261	.8000	.1960	.4498	.5547
.8500	.2044	.5182	.5337	.8500	.1935	.4472	.5853
.9000	.1787	.4808	.5325	.9000	.1839	.4328	.6067
.9500	.1536	.4433	.5240	.9500	.1678	.4087	.6207
1.0000	.1314	.4092	.5109	1.0000	.1461	.3773	.6161
1.0500	.1126	.3795	.4960	1.0500	.1204	.3413	.5894
1.1000	.0955	.3507	.4769	1.1000	.0927	.3029	.5358
1.1500	.0750	.3143	.4369	1.1500	.0655	.2635	.4549
1.2000	.0420	.2551	.3143	1.2000	.0416	.2234	.3557
SIGMA* = 0.750				SIGMA* = 0.340			
.5000	.0949	.2331	.3239	.7000	.1036	.2511	.4595
.5500	.1056	.2569	.3600	.7500	.1033	.2488	.4956
.6000	.1059	.2623	.3857	.8000	.0963	.2411	.5086
.6500	.1055	.2644	.4129	.8500	.0892	.2305	.5236
.7000	.1093	.2711	.4492	.9000	.0850	.2203	.5526
.7500	.1184	.2849	.4960	.9500	.0840	.2137	.5941
.8000	.1311	.3041	.5490	1.0000	.0843	.2120	.6327
.8500	.1440	.3242	.6009	1.0500	.0825	.2132	.6469
.9000	.1528	.3394	.6450	1.1000	.0746	.2108	.6193
.9500	.1537	.3441	.6755	1.1500	.0561	.1924	.5335
1.0000	.1439	.3338	.6861	1.2000	.0233	.1381	.3220
1.0500	.1230	.3072	.6691				
1.1000	.0939	.2671	.6156				
1.1500	.0638	.2218	.5262				
1.2000	.0451	.1869	.4609				

*Cavitation number.

TABLE 8 - CAVITATION PERFORMANCE OF PROPELLER 4738A

SIGMA* = 6.000				SIGMA* = 3.000			
J	K_T	10KQ	η	J	K_T	10KQ	η
.4500	.2358	.5204	.3245	.6000	.2350	.5097	.4404
.5000	.2808	.6114	.3654	.6500	.2449	.5327	.4755
.5500	.3029	.6592	.4022	.7000	.2530	.5510	.5115
.6000	.3077	.6752	.4352	.7500	.2542	.5583	.5434
.6500	.3000	.6687	.4641	.8000	.2463	.5520	.5681
.7000	.2837	.6472	.4884	.8500	.2297	.5327	.5833
.7500	.2621	.6163	.5077	.9000	.2065	.5032	.5877
.8000	.2377	.5799	.5218	.9500	.1794	.4670	.5807
.8500	.2123	.5408	.5311	1.0000	.1513	.4278	.5628
.9000	.1873	.5005	.5360	1.0500	.1242	.3880	.5350
.9500	.1633	.4596	.5371	1.1000	.0986	.3480	.4960
1.0000	.1404	.4181	.5344	1.1500	.0725	.3052	.4346
1.0500	.1183	.3753	.5270	1.2000	.0405	.2525	.3066
1.1000	.0963	.3302	.5104				
1.1500	.0730	.2818	.4739				
1.2000	.0468	.2291	.3904				
1.2500	.0159	.1715	.1851				
1.3000	-.0219	.1098	-.4165				
SIGMA* = 1.500				SIGMA* = 0.750			
.5000	.1002	.2497	.3194	.5000	.0841	.2072	.3230
.5500	.1081	.2634	.3591	.5500	.0976	.2392	.3572
.6000	.1259	.2964	.4056	.6000	.0990	.2436	.3880
.6500	.1470	.3366	.4517	.6500	.0974	.2392	.4213
.7000	.1663	.3753	.4938	.7000	.0982	.2372	.4611
.7500	.1807	.4063	.5308	.7500	.1033	.2430	.5074
.8000	.1881	.4261	.5620	.8000	.1123	.2571	.5564
.8500	.1877	.4330	.5865	.8500	.1231	.2764	.6024
.9000	.1797	.4269	.6031	.9000	.1324	.2959	.6410
.9500	.1649	.4089	.6096	.9500	.1369	.3093	.6690
1.0000	.1443	.3810	.6028	1.0000	.1335	.3109	.6835
1.0500	.1194	.3453	.5779	1.0500	.1207	.2965	.6802
1.1000	.0915	.3040	.5270	1.1000	.0986	.2647	.6521
1.1500	.0616	.2588	.4355	1.1500	.0702	.2184	.5888
1.2000	.0301	.2105	.2731	1.2000	.0421	.1659	.4849
SIGMA* = 0.500				SIGMA* = 0.340			
.6000	.0915	.2226	.3925	.7000	.0921	.2345	.4378
.6500	.1016	.2383	.4411	.7500	.0970	.2376	.4872
.7000	.0995	.2362	.4691	.8000	.0919	.2299	.5089
.7500	.0945	.2269	.4972	.8500	.0861	.2166	.5378
.8000	.0920	.2178	.5379	.9000	.0839	.2038	.5899
.8500	.0938	.2133	.5951	.9500	.0857	.1965	.6593
.9000	.0992	.2149	.6611	1.0000	.0891	.1972	.7192
.9500	.1056	.2215	.7207	1.0500	.0902	.2035	.7404
1.0000	.1096	.2298	.7591	1.1000	.0843	.2067	.7139
1.0500	.1078	.2344	.7683	1.1500	.0675	.1899	.6511
1.1000	.0974	.2283	.7466	1.2000	.0376	.1258	.5705
1.1500	.0772	.2028	.6970				
1.2000	.0488	.1483	.6283				

*Cavitation number.

TABLE 9 - PROPELLER OPERATING POINTS

Performance Parameters	Propeller Number			
	Design	4717B	4717C	4738A
V, knots	59.0*	59.0	59.0	59.0
J	1.037	0.942	0.982	1.010
η, rpm	1000	1103	1059	1029
η	0.67	0.52	0.62	0.72

*Rounded from 58.84.

APPENDIX A

CAVITY BOUNDARY CONDITION

From the Bernoulli equation with respect to coordinates fixed on the blade

$$\frac{P}{\rho} + \frac{q^2}{2} = \frac{P_\infty}{\rho} + \frac{V^2}{2} \tag{48}$$

where P and q are the pressure and the speed of a fluid particle relative to the blade. Thus

$$\frac{P_-}{\rho} - \frac{P_+}{\rho} = \frac{q_+^2}{2} - \frac{q_-^2}{2} = (q_+ - q_-)\ (q_+ + q_-)\ \frac{1}{2}$$
$$= G\ V_\ell \tag{49}$$

Therefore

$$\frac{\Delta P}{\frac{1}{2}\rho\ V_s^2} = \frac{2G}{V_s}\frac{V_\ell}{V_s} \tag{50}$$

Again from the Bernoulli equation

$$\frac{P-P_\infty}{\rho} = \frac{V^2}{2} - \frac{1}{2}\{(V+u_T)^2 + u_n^2\}$$

or

$$p \simeq -\frac{2V}{V_s}\frac{u_T}{V_s} = -\frac{2V}{V_s}\left(\frac{u_T^m}{V_s} + \frac{u_T^G}{V_s}\right) \tag{51}$$

This is Equation (25) or (26)

Writing

$$V_\ell = V + u_T^{(m)} + u_f \tag{52}$$

Equation (28) can be written

$$\frac{u_T^m}{V_s} = -\frac{G}{2\,V_s}\left(1+\frac{u_T^m}{V}+\frac{u_f}{V}\right)+\frac{\sigma}{2}\frac{V_s}{V}-\frac{u_f}{V_s}$$

or

$$\frac{u_T^m}{V_s}\left(2+\frac{G}{V_s}\frac{V_s}{V}\right) = -\frac{G}{V_s}\left(1+\frac{u_f}{V}\right)-\frac{2\,u_f}{V}+\sigma\frac{V_s}{V} \tag{53}$$

if $\frac{G}{V_s}$ is as small as $\frac{u_T^m}{V}$ or $\frac{u_f}{V}$, terms including $G\,u_T^m$ and $G\,u_f$ can be neglected.

APPENDIX B

LEADING-EDGE SOURCE

We assume the normal velocity on the foil cavity near the leading edge has the form

$$a_1 \frac{1}{\sqrt{x}} + a_2 + a_3 x = b_i$$

We solve for a_1, a_2, and a_3 with three points of x

$$x = 0.025,\ 0.05,\ \text{and}\ 0.1$$

$$a_1 \frac{1}{\sqrt{0.025}} + a_2 + a_3\ 0.025 = b_1$$

$$a_1 \frac{1}{\sqrt{0.05}} + a_2 + a_3\ 0.05 = b_2$$

$$a_1 \frac{1}{\sqrt{0.1}} + a_2 + a_3\ 0.1 = b_3$$

Then with the determinant

$$D = \begin{vmatrix} \frac{1}{\sqrt{0.025}} & 1 & 0.025 \\ \frac{1}{\sqrt{0.05}} & 1 & 0.05 \\ \frac{1}{\sqrt{0.1}} & 1 & 0.1 \end{vmatrix} = 0.0598745$$

we obtain

$$a_1 = (0.05b_1 - 0.075b_2 + 0.025b_3)/D$$

$$a_2 = (-0.2891b_1 + 0.5533985b_2 - 0.2044243b_3)/D$$

$$a_3 = (1.3098582b_1 - 3.1622776b_2 + 1.8524193b_3)/D$$

The total flux near the cavity is

$$\int_0^x (V_{nu} - V_{n\ell})\, dx = mx$$

mx is the flux of the corresponding wedge (or uniformly distributed V_n up to x). That is

$$m = \left| \left(2a_1\sqrt{x} + a_2x + \frac{a_3}{2} x^2 \right)_u - \left(2a_1\sqrt{x} + a_2x + a_3 \frac{x^2}{2} \right)_\ell \right| /x$$

This is the same as the leading edge cavity thickness at x

$$m = \left(2 \frac{a_1}{\sqrt{x}} + a_2 + \frac{a_3}{2} x \right)_u - \left(2 \frac{a_1}{\sqrt{x}} + a_2 + \frac{a_3}{2} x \right)_\ell$$

REFERENCES

1. Tachmindji, A.J. and W.B. Morgan, "The Design and Estimated Performance of a Series of Supercavitating Propellers," Proceedings of the 2nd Office of Naval Research Symposium on Naval Hydrodynamics, U.S. Government Printing Office (Aug 1958).

2. Venning, E. and W.L. Haberman, "Supercavitating Propeller Performance," Transactions of the Society of Naval Architects and Marine Engineers, Vol. 70 (1962).

3. Tulin, M.P., "Supercavitating Propellers - History, Operating Characteristics and Mechanics of Operation," Proceedings of the 4th Office of Naval Research Symposium on Naval Hydrodynamics, U.S. Government Printing Office (Aug 1962).

4. English, J.W., "An Approach to the Design of Fully Cavitating Propellers," American Society of Mechanical Engineers Symposium on Cavitation in Fluid Machinery (Nov 1965).

5. Pien, Pao C., "The Calculation of Marine Propellers Based on Lifting-Surface Theory," Journal of Ship Research, Vol. 5, No. 2, pp. 1-14 (Sep 1961).

6. Kerwin, J.E., "Computer Techniques for Propeller Blade Section Design," International Shipbuilding Progress, Vol. 20, No. 227 (Jul 1973).

7. Cox, G.G., "Supercavitating Propeller Theory - the Derivation of Induced Velocity," Proceedings of the 7th Office of Naval Research Symposium on Naval Hydrodynamics, U.S. Government Printing Office, pp. 929-960 (Aug 1968).

8. Luu, T.S. and P. Sulmont, "Design of Supercavitating Propellers on the Basis of Lifting Surface Theory," International Shipbuilding Progress, Vol. 16, No. 176, pp. 116-124 (Apr 1969).

9. Barr, R.A., "Supercavitating and Superventilated Propellers," Transactions of the Society of Naval Architects and Marine Engineers, Vol. 1978, pp. 417-450 (1970).

10. Scherer, J.O. and J. Bohn, "The Design of Supercavitating Propellers," Hydronautics Technical Report 7307-6 (Aug 1976).

11. Yim, B., "A Preliminary Design Theory for Polyphase Impellers in Unbounded Fluid," DTNSRDC Report 82/004 (Jan 1982).

12. Widnall, S.E., "Unsteady Loads on Supercavitating Hydrofoils of Finite Span," Journal of Ship Research, Vol. 10, No. 2, pp. 107-118 (June 1966).

13. Furuya, O., "Three-Dimensional Theory on Supercavitating Hydrofoils near a Free Surface," Journal of Fluid Mechanics, Vol. 71, Part 2, pp. 339-359 (1975).

14. Tsen, L.F. and M. Guilbaud, "A Theoretical and Experimental Study on the Planform of Supercavitating Wings," Journal of Ship Research, Vol. 18, No. 3, pp. 169-184 (Sep 1974).

15. Courant, R. and D. Hilbert, "Method of Mathematical Physics," Vol. 1, Interscience Publishers, Inc., New York, N.Y. (1953).

16. Yim, B., "Supercavitating Foil of an Arbitrary Shape Beneath or Above a Free Surface or in a Cascade," Proceedings of the Second International Conference on Numerical Ship Hydrodynamics, DTNSRDC (1977).

17. Yim, B., "Optimum Propellers with Cavity-Drag and Frictional-Drag Effects," Journal of Ship Research, Vol. 20, No. 20, pp. 118-123 (June 1976).

18. Yim, B., "A Lifting Surface Theory of Supercavitating Propellers," Proceedings for American Society of Civil Engineers-International Association for Hydraulic Research-American Society of Mechanical Engineers, Joint Symposium on Design and Operation of Fluid Machinery, Colorado State Univ. Fort Collins, Colo (June 1978).

19. Larimer, G. et al., "Experimental Investigation of the Blade-Cavity Thickness Distribution of Supercavitating Propeller 4699 and Comparison with Design Prediction,' DTNSRDC Report SPD-0801-01 (Mar 1978).

20. Baker, E.S., "Engineering Design of Two Supercavitating Propellers Using Modified Lifting Surface Programs," DTNSRDC Report SPD-680-01 (Aug 1977).

21. Christopher, K.W. and V.E. Johnson, Jr., "Experimental Investigation of Aspect-Ratio-1 Supercavitating Hydrofoils at Speeds up to 185 Feet Per Second," NASA Report TN D-787 (1960).

22. Larimer, G., "Preliminary Stress Calculations for Use in the Hydrodynamic Design of Supercavitating Propellers," DTNSRDC Report SPD-0874-03 (Nov 1979).

23. Hsu, C.C., "Some Remarks on the Progress of Cavity Flow Studies," Transactions of the American Society of Mechanical Engineers, Vol. 97, Series 1, No. 4 (Dec 1976).

INITIAL DISTRIBUTION

Copies	
2	CHONR/438
	1 R. Whitehead
	1 C.M. Lee
2	NRL
	1 Code 2027
	1 Code 2627
4	USNA
	1 Tech Lib
	1 Nav Sys Eng Dept
	1 Bhattacheryya
	1 Calisal
1	NAVPGSCOL
	1 Library
1	NADC
2	NOSC
	1 Library
	1 Higdon
1	NCEL/Code 131
13	NAVSEA
	1 SEA 031, R. Johnson
	1 SEA 031, G. Kerr
	1 SEA 031, C. Kennel
	1 SEA 05R, L. Benen
	1 SEA 05R, Lilts
	1 SEA 05R, N. Kobitz
	1 SEA 05R, J. Schuler
	1 SEA 55Y, P.A. Gale
	1 SEA 55Y, J.W. Kehoe
	1 SEA 55W, E.N. Comstock
	1 SEA 55W, R.G. Keane, Jr.
	1 SEA 6661, Blount
	1 PMS 383, Chatterton
12	DTIC
1	NSF/Engineering Lib
1	DOT/Lib TAD-491.1
1	NBS/Klebanoff

Copies	
2	MMA
	1 National Maritime Research Center
	1 Lib
1	NASA Langley Res Center/Lib
1	MARAD/Lib
3	U. of Cal/Dept Naval Arch, Berkeley
	1 Eng Library
	1 Webster
	1 Wehausen
2	U. of Cal, San Diego
	1 A.T. Ellis
	1 Scripps Inst Lib
3	CIT
	1 Aero Lib
	1 T.Y. Wu
	1 Acosta
1	Catholic U. of Amer/Civil & Mech Eng
1	Colorado State U./Eng Res Cen
1	Florida Atlantic U.
	1 Tech Lib
1	U. of Hawaii/St. Denis
1	U. of Illinois/J. Robertson
2	U. of Iowa
	1 Library
	1 Landweber
1	U. of Kansas/Civil Eng Lib
1	Lehigh U./Fritz Eng Lab Lib
3	MIT
	1 Ogilvie
	1 Leehey
	1 Kerwin

Copies	
2	U. of Mich/NAME 1 Library 1 Benford
1	U. of Notre Dame 1 Eng Lib
2	Penn State ARL 1 Lib 1 B. Parkin
1	U. of Minnesota/Song
2	New York U./Courant Inst 1 A. Peters 1 J. Stoker
2	SIT 1 Breslin 1 Tsakonas
1	U. of Texas/Arl Lib
2	Southwest Res Inst 1 Applied Mech Rev 1 Abramson
1	Stanford Res Inst/Lib
1	U. of Washington 1 Eng Lib
2	Webb Inst 1 Library 1 Ward
1	Woods Hole/Ocean Eng
1	SNAME/Tech Lib
1	Bethlehem Steel/Sparrows Point
1	General Dynamics, EB/Boatwright
1	Gibbs & Cox/Tech Info

Copies	
4	Hydronautics 1 Library 1 M. Tulin 1 C. Hsu 1 V. Johnson
1	Lockheed, Sunnyvale 1 Potash
1	Newport News Shipbuilding/Lib
1	Oceanics
1	Boeing Company/Seattle 1 Marine System
1	Grumman Aerospace/W. Carl
1	Sperry Rand/Tech Lib
1	Sun Shipbuilding/Chief Naval Arch
1	American Bureau of Shipping 1 Lib
1	Maritime Research Information Service

CENTER DISTRIBUTION

Copies	Code	Name
1	1170	G.R. Lamb
1	1170	S. Hawkins
1	012	B.V. Nakonechny
1	012	D. Jewell
1	012	R.M. Stevens
1	1500	W.B. Morgan
1	1504	V.J. Monacella
1	1506	J.A. Fein
1	1520	W.C. Lin
1	1521	W.G. Day
1	1522	G.F. Dobay
1	1522	M.B. Wilson
10	1522	J.G. Peck

Copie	Code	Name
1	1540	J.H. McCarthy
10	1540	B. Yim
1	1542	T.T. Huang
1	1544	T.E. Brockett
10	1544	G.E. Larimer
1	1560	D. Cieslowski
1	1561	G.G. Cox
1	1561	S.L. Bales
1	1562	D.D. Moran
1	1562	E.E. Zarnick
1	1563	W.E. Smith
1	1564	J.P. Feldman
1	1840	J. Schot
10	5211.1	Reports Distribution
1	522.1	Unclassified Lib (C) 1(m)
1	522.2	Unclassified Lib (A)